ISAS - INTERNATIONAL SCHOOL FOR ADVANCED STUDIES

River Networks Dynamics, Branching Patterns and Aggregation Phenomena.

Thesis submitted for the degree of
"Doctor Philosophiæ"

CANDIDATE

Francesca Colaiori

SUPERVISOR

Prof. Amos Maritan

October 1996

SISSA - SCUOLA INTERNAZIONALE SUPERIORE DI STUDI AVANZATI
TRIESTE
Strada Costiera 11

TRIESTE

Table of Contents

List of Figures

1 Introduction

Lot of complex structures can be characterized using the concepts of fractal geometry. The key point leading to this description is the recognition that these structures obey a striking kind of symmetry, the *scale invariance*, implying that these objects look the same on different scales of observation. Examples of these kind of structures can be found in various field of science, and on various scales. Clouds, landscapes, lightnings, fractures and galaxies are all fractal objects.
Researches in the fields of diffusion-limited reactions and surfaces growth demonstrated that scaling concepts, similar to those successfully developed in the context of phase transitions in equilibrium statistical mechanics, could provide a powerful technique in the study of scale invariant systems.

The main part of this work deals with a rather unusual subject in non-equilibrium statistical mechanics, that is the **dynamics of river networks.**
Many laws of Nature are independent, or nearly so, of a scaling factor, reflecting the fact that, as observed previously, many structures observed in Nature are *self-similar*, i.e. invariant against changes in scale. River networks are a beautiful example of such self-similar structures, and their fractal character can be observed experimentally on several scales.
Previous approaches to the problem focused especially on reproducing the statistical characteristics of the drainage network, without taking care of the dynamic driving these systems in their critical state.
We propose a model which is able to predict the final stable shape of the landscape obtained, as a product of erosion, from an initially featureless surface.
The equation for the landscape evolution is derived from very simple principles, and, in spite of that, provides a good explanation for all observed facts in geomorphology. Moreover, it predicts the exact scaling of a new quantity that may be deduced from observational data and that will thus provide a decisive test for our theory.

Another reason for being interested in drainage networks comes from the fact that they provide a beautiful example of *tree-like* structures spontaneously produced in Nature.
Branching patterns abounds in Nature. Examples can be found everywhere: in blood

vessels, Lichtenberg figures created by dielectric breakdown, crystal aggregates, patterns generated by viscous fingering, even in termite trails in sand! Some of these fascinating patterns are shown in fig. 1.1, 1.2 and 1.3.
A desirable goal would be to characterize these patterns and understand what leads to them.
In the case of the river networks we will see that loopless structures arise quite naturally from the minimization of the dissipated energy under the constraint of the continuity equation for the flow.

The last part of this work will deal with random aggregation models and reaction diffusion processes.
We will show that a much studied random aggregation model proposed by Takayasu (equivalent to one of the first river networks models proposed by Scheiddeger!) can be mapped on the diffusive annihilation. This random aggregation model was already known to be related to the directed sand-piles and to the voter model, that is a stochastic model for the formation of public opinion.
Finding an exact mapping between various problems of physics always represent an important progress, from which all them may benefit.

CAPTIONS:

(1.1 a) Aggregates of zinc from an experiment of metal crystalline deposit growth.
(1.1 b) Branching patterns in an experiment of viscous fingering.
(1.2 a) Lichtenberg patterns created by dielectric breakdown.
(1.2 b) Pattern of termite trails searching food in sand.
(1.3 a) Radar image of the Mississippi River delta.
(1.3 b) Radar image of Mount Rainier in Washington state. At the top of the image curving to the northwest you can see the White River, leaving the mountain at the bottom right (south) Nisqually River, and leaving to the left the Carbon river.

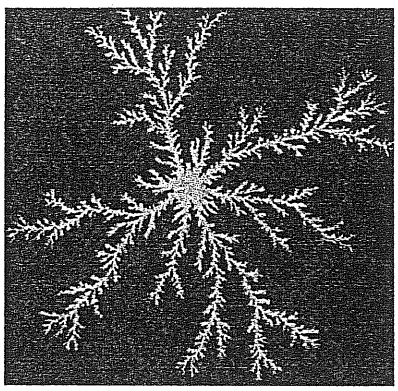

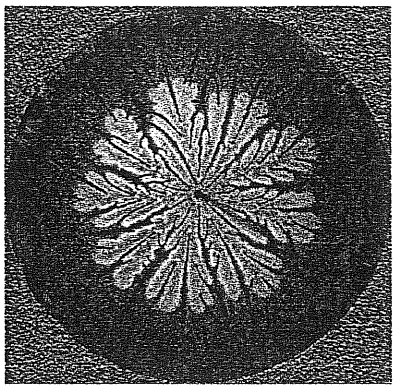

Figure 1.1: (a) (b)

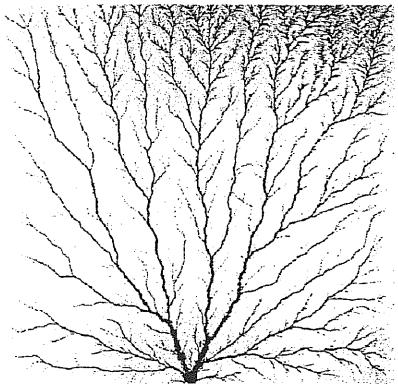

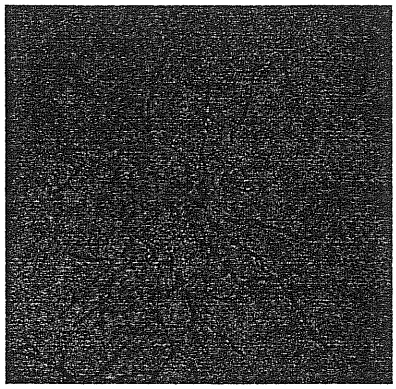

Figure 1.2: (a) (b)

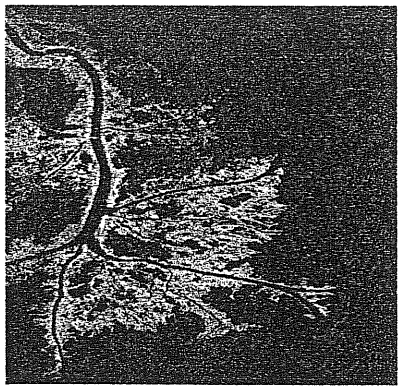

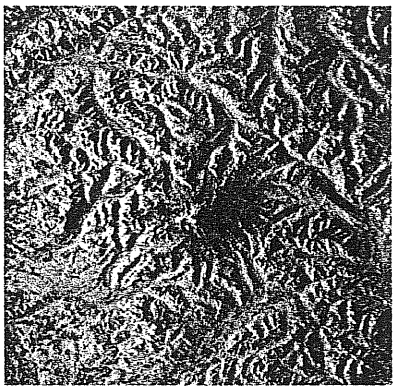

Figure 1.3: (a) (b)

2 Dynamics of River Networks

The numerous efforts to model river networks [3, 4, 5] have primarily focused on reproducing the statistical characteristics of the drainage network. Less attention has been payed to the temporal behaviour and to the evolution of the profile. Some previous models have been proposed by [6, 7, 8, 9] but none of them is capable to predict the shape of the final profile obtained when erosion keeps acting on an initially featureless surface.

In this chapter we present a nonlinear model which describes the evolution of a landscape under the effects of erosion by means of a simple differential equation. The equation is derived by reparametrization invariance arguments [10, 11] and exactly solved in $d = 1$. Results of numerical simulations in $d = 2$ show that the model is able to reproduce not only qualitatively but also quantitatively the critical scaling characterizing landscapes observed in natural river basins. We also predict the exact scaling of a quantity that may be deduced from experimental observations, providing a test of our theory.

The chapter is organized as follows: in the first section we introduce the reader to this rather unusual topic of non-equilibrium statistical mechanics, defining what is called *river basin*, what kind of data are available from Nature, and what are the experimentally observed facts. Then we introduce the equation for the for the evolution of a basin's landscape, deducing it from simple principles.
In section 2 we show how the equation proposed to describe the evolution, can be regarded as a lower order gradient expansion of an equation obtained by reparametrization invariance arguments [12, 11].
We solve exactly the equation in $d = 1$ (section 3) showing that it is equivalent to the Burgers equation [13] without viscosity. The solution in one dimension not only gives some qualitative features of the two dimensional case, but can be interpreted as the evolution along the mainstream in the physical case ($d = 2$) if one takes properly into account the area collected by each point of this stream. Moreover the $d = 1$ case turns out to be enlightening about the role of boundary conditions.
Results of a numerical analysis in $d = 1$ are presented in section 4 both in the deterministic case and in the case in presence of multiplicative disorder, modeling a random rainfall.

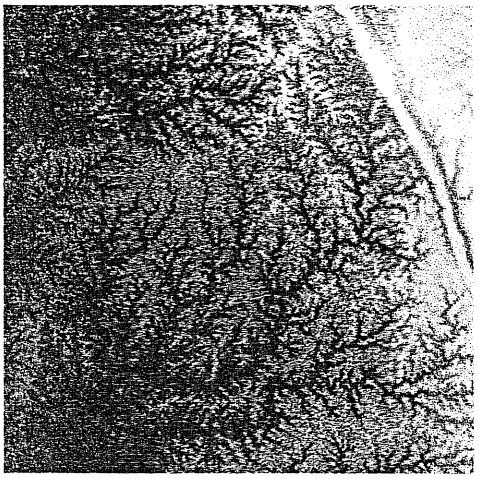

Figure 2.1: Subbasin of the Kentucky River basin. Kentucky makes a good study region because there are few geologic controls and the climate is fairly homogeneous and humid throughout the region. The predominant lithology of the bedrock in this region is limestone. DEM image: The lowest elevations are red and black, while the highest ones are yellow and white. The white diagonal stripe near the bottom is Pine Ridge, which also shows up well on the shaded aspect image.

In section 5 we briefly reviewed the finite size scaling ansatz proposed in [10] describing the critical behaviour exhibited by river network models and the scaling laws [14] relating the critical exponents. Results of numerical studies in $d = 2$ are reported in section 6. Simulations have been performed both by direct integration of the equation and with the help of a new algorithm converging very quickly to stationary solutions. The latter method allows to get very good statistics. Critical behaviour of stationary solutions is analyzed in details in the context of the finite size scaling ansatz, showing a perfect consistency with already known scaling relations and a very good qualitative and quantitative agreement with real data.

Numerical results reported in section 7 refers to simulations obtained "heating" the system with an additive noise term and then carefully quenching. The aim is to reach more stable solutions. The motivations come from the fact that stationary solutions of the evolution equation are strictly related to the solutions of an optimization problem arising from a static model of river networks [15, 16], and will become clear in the next chapter. With this method we found a distinct class of stationary solutions whose critical behaviour is characterized by a different set of exponent corresponding to a mean field model [17].

Results of numerical studies in $d = 2$ in presence of multiplicative correlated and uncorrelated noise, again modeling randomness in the rainfall are reported in section 8.

All the results obtained are summarized and discussed in section 9.

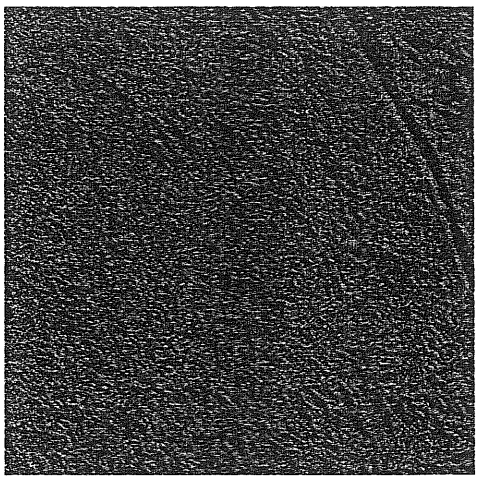

Figure 2.2: A shaded aspect image. In this image, each pixel's color is determined by the direction in which water would flow away from that pixel.

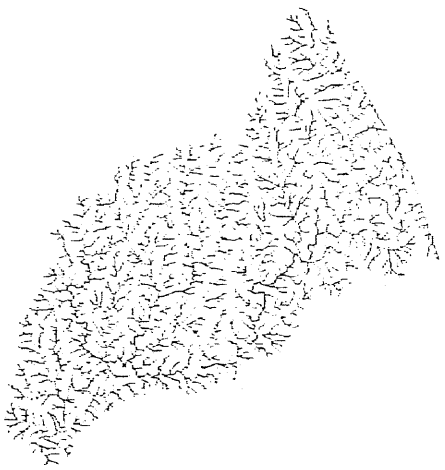

Figure 2.3: A river network image. The colors in this image blue, green, yellow, orange, red, and black correspond to streams of different *Stralher orders* [1, 2]. Stralher ordering system is the most common classification scheme of the hierarchical branching structure of river networks used in hydro-geomorphology.

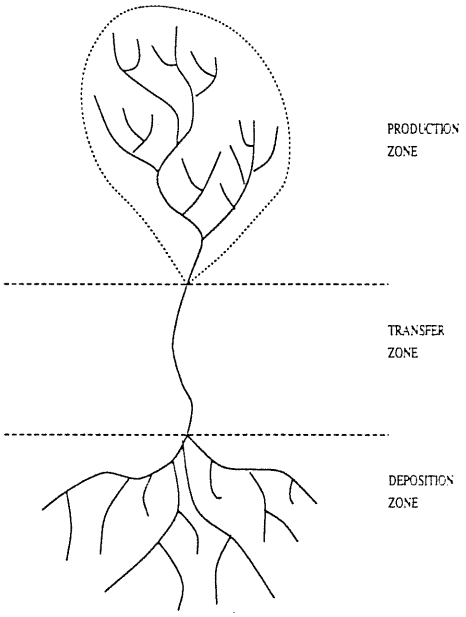

Figure 2.4: Idealized fluvial system. The region inside the dotted line is the drainage basin.

2.1 General Framework

Branched river networks are one of the most common examples of fractal patterns spontaneously produced in Nature. Examples are shown in figures 2.1, 2.2 and 2.3 relative to a sub-basins of the Kentucky river basin. The three images comes from processing of data from satellite. The drainage network in a river basin has a tree-like structure which provides an efficient means of transportation. Experimental analysis on river basins have shown clear evidences of fractal behaviour characterized by the absence of a single well-defined length scale.

2.1.1 Definitions and Empirical Observations

A fluvial system may be ideally divided in three distinct regions (see fig 2.4). They are called according to their working purpose *production zone*, *transfer zone* and *deposition zone* [18].

We call **river basin** the production zone of a river that is where water is collected.

Data relative to the landscape of a basin are available from *Digital Elevation Maps* (DEM) [19, 20] consisting in discretized elevation fields obtained by topography from space. The unitary areas in the discretization units are called *pixels* and are boxes of about $30 \times 30m$ in a square grid. The drainage network is determined from a DEM assigning to each pixel a drainage direction. Since water flows downhill through the steepest descent, drainage

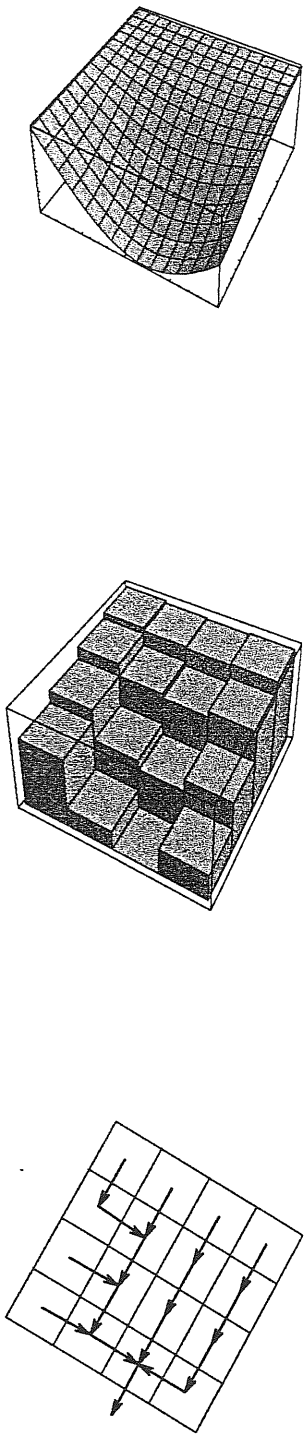

Figure 2.5: The construction of the river network from the landscape in a simple example.

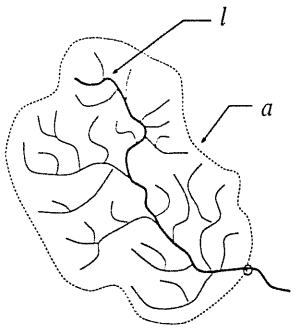

Figure 2.6: Hack law relates the length of the mainstream in the (sub-)basin with the total area of the (sub-)basin.

directions go from each pixel to the nearest neighbour with the lowest height. Multiple flow directions are excluded since they practically do not occur in Nature, at least in the production zone. Figure 2.5 shows how construct the drainage network from the landscape in a simple example.
To each pixel i one can associate a variable that gives the number of pixels draining through i. This quantity represents the total drainage area (**cumulated area**) a_i at the point i expressed in pixel units, and, in the case of uniform rainfall, provides a measure of the flow at that point. The **upstream length** l_i at the point i is defined as the distance from the farthest source draining in i, measured along the stream.
In a first approximation channels may be defined as made of those pixels with total drainage area greater than a support area threshold even if it has been argued [21] that support area alone may not be sufficient to determine channels initiation.

Observations lead to a lot of empirical relations between quantities characterizing rivers morphology. The *Hack's law* (1957) [22], relates the length of the leading stream l in a drainage region with the area a of that region (see 2.6): $l = ka^h$ with $k \simeq 1.4$ and $h \simeq 0.6$. In fig. 2.7 some experimental data from [22] are shown. This relation is true both for sub-basins of the same basin (fig 2.7 (A)) and for the whole basin of different rivers (fig 2.7 (B)) with the same approximative values for k and h.
The sensitive departure of the observed value of $h \simeq 0.6$ from the Euclidean value $\frac{1}{2}$ lead to the first conjectures about the fractality of rivers [23].

Another well established empirical relation (*slope-discharge*) is between the flow in a point and the gradient of the height of the landscape at that point (see fig. 2.9): $\mid \vec{\nabla} h \mid \propto J^{\gamma-1}$ with a numerical value of γ around 0.5.

The distributions of accumulated ares a_i and upstream length l_i are characterized by power law distributions with exponents τ and ψ respectively, in the ranges $1.42 - 1.46$, $1.73 - 1.85$.

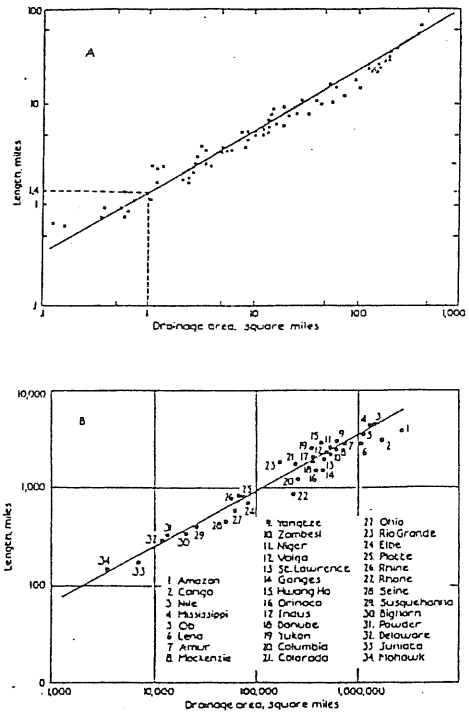

Figure 2.7: Figure (A) shows the relation between length of the longest stream and drained area in different sub-basins of the same basin (Shenandoah Valley, Virginia). Figure (B) shows the relation between mainstream and total drained area for different rivers in different parts of the world.

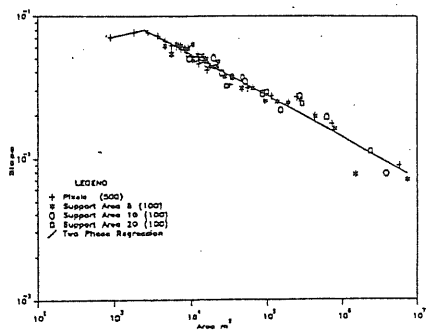

Figure 2.8: Log-log plot of slope versus discharge (with different DEM support areas) for Hack basin (Schoharie Creek headwaters, Hunter, NY).

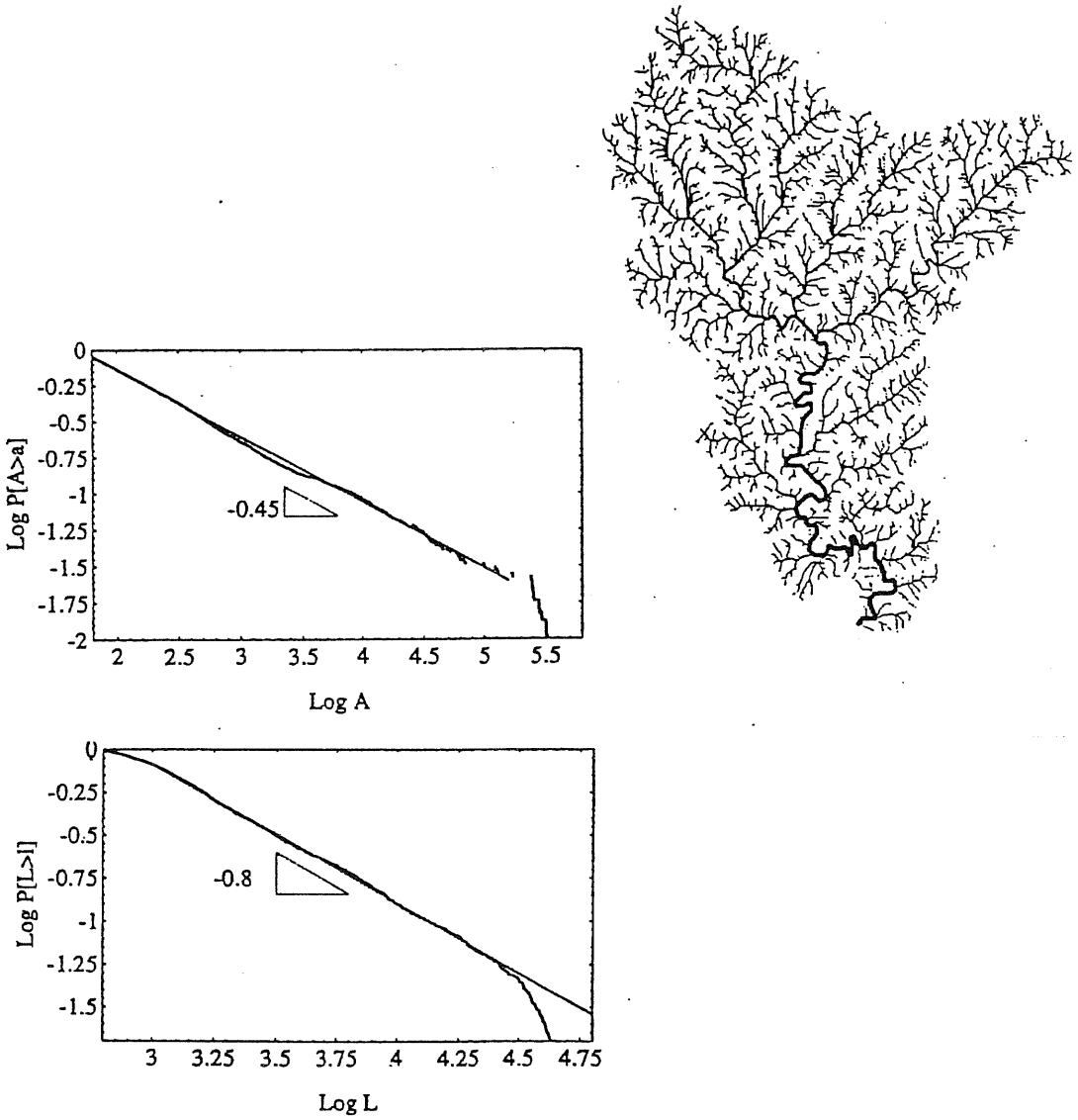

Figure 2.9: DEM of Brushy River, probability distributions of cumulated areas and upstream lengths are shown in log-log plots, and the corresponding exponents are $\tau \approx 1.45$ and $\psi \approx 1.80$.

2.1.2 Equation for the Evolution of a Landscape under the Effects of Erosion

Recently a lot of efforts have been done in order to define static models able to reproduce the previous mentioned statistical characteristics of real rivers (for a review see [24]).

Real drainage basins are not static but evolve on extremely long time scales. Nevertheless some statistical properties seems to be preserved during the evolution. This consideration follows from the fact that some quantities characterizing river basins morphology are almost the same for all rivers, irrespectively of their "age".

Our aim is to find the simplest model that simulates an evolution to morphologically realistic landscapes and that preserve certain features during evolution. The equation we propose to describe the evolution of the landscape is

$$\dot{Z}(t,\underline{x}) = -\alpha J(t,\underline{x}) \mid \vec{\nabla} Z(t,\underline{x}) \mid^2 + \gamma \nabla^2 Z(t,\underline{x}) + c\,, \tag{2.1}$$

where Z denotes the elevation in the point $\underline{x} = (x,y)$ of the substrate plane at time t and $J(t,\underline{x})$ the modulus of the flux in that point at time t. The first term is an erosional term proportional to the flux, the second is a diffusive term and the third is a constant term modeling a constant *uplift*. The existence of an uplift originated by tectonic forces is a well known fact in geomorphology [21, 25]: a landscape represents the instantaneous equilibrium of two concurrently active processes, uplift (endogenic) and degradation (exogenic). A stationary state results from the exact balance of this two agents.

A simple argument leading to an equation of the form (2.1) is the following: the evolution of a landscape had to be of the form $\dot{Z} = F(\vec{\nabla} Z, \nabla^2 Z, ..., J)$, where an explicit dependence on Z is excluded since would break the translational invariance, and the dependence on $\vec{J}$ (bidimensional projection) is simply trough $J = \mid \vec{J} \mid$ since $\vec{J} \parallel \vec{\nabla} Z$. In the small gradients expansion

$$\dot{Z} = A + \vec{B} \cdot \vec{\nabla} Z + C(\vec{\nabla} Z)^2 + \cdots . \tag{2.2}$$

Observing that in order to ensure the rotational invariance it must be $\vec{B} = 0$, one recovers an equation of the form (2.1). In the next section equation (2.1) will be derived by reparametrization invariance.

The constant term in equation (2.1) can be eliminated by simply replacing $Z(t,\underline{x})$ with $z(t,\underline{x}) = Z(t,\underline{x}) - ct$. In what follows we will always consider the frame in which the system drifts with velocity c an thus equation (2.1) can be rewritten as

$$\dot{z}(t,\underline{x}) = -\alpha J(t,\underline{x}) \mid \vec{\nabla} z(t,\underline{x}) \mid^2 + \gamma \nabla^2 z(t,\underline{x})\,. \tag{2.3}$$

The diffusive term act on the surface even in points with infinitesimal contributing areas where the first term vanishes since the flux become zero. In absence of the diffusive term

the presence of maxima on the surface will cause the formation of singularities during the evolution, since points at the top of an hill will never be eroded by the first term (both J and $\vec{\nabla} z$ vanish). The presence of even an infinitesimal diffusive term is then essential in eliminating these singularities.

In the discretized version of the model each site (pixel) collect at least an unit area, thus no singularities due to a vanishing contributing area appear even in absence of the diffusive term . Moreover the discretization introduce implicitly a diffusive term since it smoothes z on distances of the order of the lattice length and then prevent also from singularities due to a vanishing $\vec{\nabla} z$ that appear when $\gamma = 0$.

For these reasons we will focus on the simplified version of equation (2.3) in its lattice discretization obtained by putting $\gamma = 0$. In fact, due to the coarse grained scale of the elevations field, the effects of the diffusive term would be negligible. The possible relevance of that term will be discussed later.
In this case the equation reduces to

$$\dot{z}(t, \underline{x}) = -a J(t. \underline{x}) \mid \vec{\nabla} z(t, \underline{x}) \mid^2 . \tag{2.4}$$

When it is not explicitly stated the flux is taken to be proportional to the drained area and flux and drained areas are used indifferently. This corresponds to have an uniform rainfall acting on the surface.

In spite of its simplicity, this model shows a lot of interesting features.
The stationary solutions of equation 2.4 are such that

$$\mid \vec{\nabla} z \mid \propto J^{-1/2} . \tag{2.5}$$

This the previous mentioned *slope-discharge* relation and is a well known empirical fact.

It will be shown that the evolution is characterized by two time scales. The elevations are lowered in a nonuniform way by erosion, causing variations of the draining directions during the evolution. Sketching again the system with a lattice model, one can associate to any time a two dimensional configuration giving the drainage directions at any site (fig. 2.5). After a first characteristic time, the *freezing time*, the spanning graph determining the two dimensional configuration of the basin does no longer changes. Erosion keeps acting (till equation (2.5) holds at any site) on the profile but preserves the two dimensional drainage structure. The second characteristic time, much longer, is the *relaxation time* at which the profile reaches its stable shape.

Since a lot of the measured quantities like the distributions of drained areas and mainstream lengths depend only on the two dimensional structure, the existence of a freezing time much smaller than the relaxing time may provide an explanation of the phenomena we were pointing out at the beginning, that is the fact that some statistical properties must be preserved during the evolution since are found to be almost the same for all rivers.

2.2 Evolution Equation for River Networks by Reparametrization Invariance

The evolution of a surface under the effect of erosion can be described in terms of an equation of the form

$$\partial_t \vec{r}(\underline{s},t) = \hat{n}(\underline{s},t)\mathcal{F}[\vec{r}(\underline{s},t), \vec{J}(\vec{r}(\underline{s},t)), \vec{G}] \tag{2.6}$$

where $\vec{r}(\underline{s},t)$ is a three dimensional vector spanning the surface and $\underline{s} = (s_1, s_2)$ varies in a parameter space. $\hat{n}(\underline{s},t)$ is the unit normal to the surface at $\vec{r}(\underline{s},t)$, $\vec{G}$ is the gravitation field supposed to be constant on the surface, $\vec{J}(\vec{r}(\underline{s},t))$ is the flux in the point $\vec{r}$ which is directed along the steepest descent direction of the surface and $\mathcal{F}$ contains a deterministic erosional mechanisms. The time derivative of $\vec{r}$ must be parallel to the normal to the surface. This follows by regarding $t = s_0$ as a coordinate in a curvilinear coordinate system (s_0, s_1, s_2). Changes of the parametrization cannot involve s_0, since it represent the absolute time. This implies that the elements $g_{0,i} = \partial_0 \vec{r} \cdot \partial_i \vec{r}$ of the metric tensor vanish. Thus it must be $\partial_0 \vec{r} \perp \partial_i \vec{r}, \forall i$, i.e. $\partial_t \vec{r}$ is perpendicular to the plane tangent to the surface in $\vec{r}$ and then $\vec{r} \parallel \hat{n}$.

With general considerations one can guess the form of $\mathcal{F}$. The first is the reparametrization invariance: irrespectively of the details driving the evolution, the equation must satisfy the requirement to be independent of the choice of the particular parametrization, $\underline{s}$, we are using to describe the surface. This means that the only quantities that can enter in the equation are intrinsic i.e. invariant under reparametrization.

The second consideration is that in absence of flux, erosion does not take places, and then $\partial_t \vec{r}$ must be equal to zero. Calling J the modulus of the flux, the simplest hypothesis is:

$$\mathcal{F} = J\tilde{\mathcal{F}} + \mathcal{O}(J^2)\,. \tag{2.7}$$

$\tilde{\mathcal{F}}$ is a scalar, thus it must depend by $\hat{n}$ and $\vec{G}$ only by their scalar product $\hat{n} \cdot \vec{G}$. Moreover, when $\hat{n} \parallel \vec{G}$ again no erosion must take place, thus $\tilde{\mathcal{F}} = 0$. This suggest:

$$\tilde{\mathcal{F}} = G + \hat{n} \cdot \vec{G} \tag{2.8}$$

where G denotes the modulus of $\vec{G}$.

Thus, to the first order in J

$$\mathcal{F} = J(G + \hat{n} \cdot \vec{G}) \tag{2.9}$$

Let us use for $\vec{r}$ the Monge parametrization. In the Monge parametrization $\underline{x}$ is a two dimensional vector in the "substrate" plane and $z(\underline{x})$ is the height of the surface in the direction z ($\parallel \vec{G}$) perpendicular to that plane. This is not the most general parametrization: the presence of overhangs in the surface is in fact excluded, otherwise the function $z(\underline{x})$

would no more be single valued. Nevertheless it is enough general for our purposes. In this parametrization the metric tensor has the form $g_{ij} = \delta_{ij} + \partial_i z\, \partial_j z$ with determinant $g = 1 + |\vec{\nabla} z|^2$. The normal versor is

$$\hat{n} = g^{-1/2} \partial_i \vec{r} \times \partial_j \vec{r} = \frac{(-\vec{\nabla} z, 1)}{\sqrt{1 + |\vec{\nabla} z|^2}}. \tag{2.10}$$

In these coordinates, equation (2.6) reads

$$\partial_t \vec{r}(\underline{x}, z(\underline{x}, t)) = \hat{n}(\underline{x}, z(\underline{x}, t)) \mathcal{F}. \tag{2.11}$$

Taking in both sides the scalar product with the versor $\hat{n}$ yield

$$\dot{z} = \mathcal{F} \sqrt{1 + |\vec{\nabla} z|^2}. \tag{2.12}$$

Thus $\frac{\dot{z}}{\sqrt{1+|\vec{\nabla} z|^2}}$ has the meaning of velocity in the direction perpendicular to the surface. Replacing in equation (2.12) the expression of $\mathcal{F}$ given by equation (2.9) and using $\vec{G} = G(0, 0, 1)$

$$\dot{z} = GJ(\sqrt{1 + |\vec{\nabla} z|^2} - 1). \tag{2.13}$$

To the lowest order in the gradient expansion equation (2.4) is recovered.

2.3 Analytic Solution in $d = 1$

Equation (2.4) in $d = 1$ determines uniquely the evolution of a profile $z(t)$ once boundary conditions are properly chosen. We will study the equation on a segment $[0, L]$. The initial profile $z_0(x)$ and the elevation in L at any time determine uniquely the solution. In what follows, in particular, we will consider the case in which the point at L lowers with constant velocity v. We will show that this equation has a stationary solution in the sense that after a certain relaxing time the profile will rigidly move with the constant velocity v preserving its shape. This is exactly the solution we are interested in, since it is constant in time in the real coordinates $Z(x, t) = z(x, t) + ct$ if the velocity v is taken equal to the uplift c. For smooth profiles without lakes $J = x$ and then equation (2.4) becomes

$$\dot{z}(x, t) = -x[\partial_x z(x, t)]^2, \qquad x \in [0, L] \tag{2.14}$$

with boundary conditions

$$\begin{cases} z(x, 0) = z_0(x) \\ \dot{z}(L, t) = -v \qquad (v > 0). \end{cases} \tag{2.15}$$

With the change of variable $y = \sqrt{x}$ and deriving both sides with respect to x one gets an equation for $u(y, t) = \partial_y \tilde{z}(y, t) = 2\sqrt{x} \partial_x z(x, t)\,|_{x=y^2}$:

$$\dot{u}(y, t) = -\frac{1}{2} u(y, t) \partial_y u(y, t) \tag{2.16}$$

with boundary conditions

$$\begin{cases} u(y,0) = u_0(y) = 2y(\partial_x z_0(x))\,|_{x=y^2} \\ u(\sqrt{L},t) = -2\sqrt{v}\,. \end{cases} \tag{2.17}$$

Note that the boundary conditions (2.17) give rise to a continuous solution only if $u_0(\sqrt{L}) = -2\sqrt{v}$ i.e. if $\partial_x z_0(x)\,|_L = -\frac{\sqrt{v}}{\sqrt{L}}$. In effect we will show that the discontinuity in $u(y,t)$ does not imply a discontinuity in $z(x,t)$ if the initial condition z_0 is such that $\partial_x z_0(x)\,|_L \geq -\frac{\sqrt{v}}{\sqrt{L}}$.

Equation 2.16 is the Burger [13] equation without the viscosity term. This is a special case of a class of differential equations called *conservation laws* and related to the problem of shock waves that have been extensively studied both from physicists and mathematicians. Their solution is well known on $(-\infty,\infty)$. We will show that the problem on $[0,L]$ defined by equation (2.16), with boundary conditions (2.17), is equivalent to a certain problem on $(-\infty,\infty)$ and can be thus solved exactly.

The general solution of equation (2.16) is implicitly given by (see for example [26], Cap. 15)

$$u(y,t) = \hat{u}_0\Big(y - \frac{1}{2}tu(y,t)\Big) \tag{2.18}$$

where u_0 is a suitable initial condition[1]. This can be checked quite easily by direct substitution in equation (2.16). If boundary conditions are supposed in the form

$$\begin{cases} u(y,0) = u_0(y) & 0 \leq y \leq A \\ u(A,t) = f(t) & t \geq 0 \end{cases} \tag{2.19}$$

where u_0 and f are specific known functions, then

$$\hat{u}_0(y) = \begin{cases} u_0(y) & 0 \leq y \leq A \\ 2\frac{A-y}{t(y)} & y \geq A \end{cases} \tag{2.20}$$

where $t(y)$ solves the equation $y = A - \frac{1}{2}tf(t)$. f must be such that equation (2.20) does not contains ambiguity in the definition of u_0. In the specific case of equation (2.17) $f = const = -2\sqrt{v}$, equation (2.20) becomes

$$\hat{u}_0(y) = \begin{cases} 2y(\partial_x z_0(x))\,|_{x=y^2} & y \in [0,\sqrt{L}) \\ -2\sqrt{v} & y \geq \sqrt{L} \end{cases} \tag{2.21}$$

and thus, trough equation (2.18), we have the complete solution for $z(x,t), \forall t > 0$, which taking into account equation (2.15) becomes

$$z(x,t) = -\int_x^L \frac{dx'}{2\sqrt{x'}} u(\sqrt{x'},t) - vt\,. \tag{2.22}$$

[1] One can show that the only C^1 functions which satisfy equation (2.16) for any $t \geq 0$ are those which are monotonically *increasing* in y for each fixed $t \geq 0$. Our u_0 is not an increasing function and the solution on $y \in (0,\infty)$ exist only up to time $t = -1/u_0'$. However, the solution on $[0,L]$ remain finite for any $y \in (0,L]$. However, u_0 cannot be arbitrary. A sufficient condition for the existence of the solution for any $t \geq 0$ for the problem on $[0,L]$ with a decreasing initial condition u_0 is for example that $u_0'' \geq 0$.

Such solution depends on the initial profile z_0 only in the transient regime, while the stationary solution depends only on v.
For example, if the initial condition is simply a line with slope $-m$: $z(x,0) = m(L-x)$, from the above equations one easily finds

$$z(x,t) = \begin{cases} -\frac{mx}{1-mt} + mL & x < \bar{x}(t) \\ 2\sqrt{v}(\sqrt{L} - \sqrt{x}) - vt & x \geq \bar{x}(t) \end{cases} \tag{2.23}$$

where the function $\bar{x}(t)$ must be determined imposing the continuity of z. Such function exists for any $m \leq \frac{\sqrt{v}}{\sqrt{L}}$ and it is given by

$$\bar{x}(t) = \frac{(1-mt)}{m^2}\left(\sqrt{v} - \left(\frac{\sqrt{v} - m\sqrt{L}}{\sqrt{1-mt}}\right)\right)^2 \tag{2.24}$$

In this case it emerges quite clearly a relaxation time for the evolution that could be defined as

$$t_R = \max_{x\in[0,L]} \bar{t}(x)\,. \tag{2.25}$$

where $t = \bar{t}(x)$ is the inverse function of $x = \bar{x}(t)$.
In the simple case of equation (2.23), $t_R = 2\frac{\sqrt{L}}{\sqrt{v}} - \frac{mL}{v}$. If $m = \epsilon\sqrt{\frac{v}{L}}$ with $0 \leq \epsilon \leq 1$ then $t_R = \sqrt{\frac{L}{v}}(2-\epsilon) \sim \sqrt{\frac{L}{v}}$.
For a generic initial condition $t_R \sim \sqrt{L}$.
The last statement can be easily obtained with the following scaling argument: assuming the scaling of x, z and t with L:

$$x \sim L \quad , z \sim L^{\alpha} \quad , t \sim L^{\zeta}\,, \tag{2.26}$$

one gets, from equation (2.14) that $\alpha - \zeta = 2\alpha - 1 = 0$ and then

$$\alpha = \zeta = 1/2\,. \tag{2.27}$$

The solution $z(x,t,L)$ assumes the scaling form

$$z(x,t,L) = \sqrt{L} f\left(\frac{x}{L}, \frac{t}{L^{\zeta}}\right), \tag{2.28}$$

where f is a scaling function given by

$$f(w,k) = -\int_w^1 \frac{ds}{2\sqrt{s}} \bar{u}(\sqrt{s},k) - vk\,, \tag{2.29}$$

where $\bar{u}(\sqrt{\frac{x}{L}}, \frac{t}{\sqrt{L}}) = u(\sqrt{x}, t; L)$ and we used the fact that the function $u(\sqrt{x}, t; L)$ can be expressed in terms of the dimensionless variables $w = \frac{x}{L}$ and $k = \frac{t}{\sqrt{L}}$. This is possible since from equation (2.18) $u \sim L^{\frac{1}{2}-\zeta} = L^0$ (equivalently, from the definition of u, $u \sim L^{\alpha-\frac{1}{2}}$).
For $t \geq t_R$ the scaling function becomes $f(w,k) = 2\sqrt{v}(1-\sqrt{w}) - vk$.

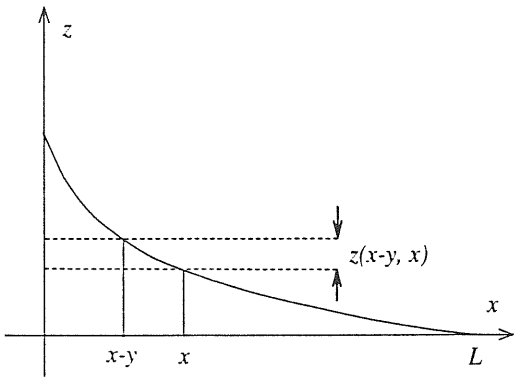

Figure 2.10: Alternative derivation for the form of the scaling function f.

This scaling argument is also useful to analyze the relevance of a possible diffusive term $\partial_x^2 z$ in the equation. Such term should scale as $L^{\alpha-2} = L^{-3/2}$ and then results to be irrelevant in the large size limit.

Note that the presence of the uplift in equation (2.1) is essential to avoid a constant down drift of the landscape and the flattening of the landscape. In fact the stationary solution

$$z(x,t) = 2\sqrt{v}(\sqrt{L} - \sqrt{x}) - vt \tag{2.30}$$

vanishes if $v = 0$. This is indeed what happens for the particular choice of ref. [7].

It is interesting to note that the form of the scaling function in the stationary solution (2.30) can be obtained from very general considerations and on the scaling assumption, without referring to a specific evolution equation. For a river of size L let $z(x, L)$ be the hight at position x. We impose $z(L, L) = 0$. The height $z(x - y, L)$ with $y > 0$ can be related to the height $z(x, L)$ and to the one of a river of length x at position $x - y$ as follows (see fig. 2.10):

$$z(x - y, L) = z(x, L) + z(x - y, x)\,. \tag{2.31}$$

In the limit $y \to 0$

$$z(x, L) - yz_1'(x, L) = z(x, L) + z(x, x) - yz_1'(x, x) \tag{2.32}$$

where $z_1'(x, L) = \frac{\partial z}{\partial x}(x, L)$. From equation (2.32), being $z(x, x) = 0$, it follows $\frac{\partial z}{\partial x}(x, L) = z_1'(x, x)$ independent of L. Integrating $\frac{\partial z}{\partial x}(x, L)$ from 0 to L we have

$$z(L, L) - z(x, L) = \int_x^L \frac{\partial z}{\partial s}(s, L)ds = \int_x^L z_1'(s, s)ds = F(L) - F(x)\,. \tag{2.33}$$

where F is a primitive of z_1' i.e. $\frac{\partial F}{\partial x}(x) = z_1'(x, x)$. Since $z(L, L) = 0$, we have $z(x, L) = F(x) - F(L)$. This is the general expression that a profile must have (up to this point we

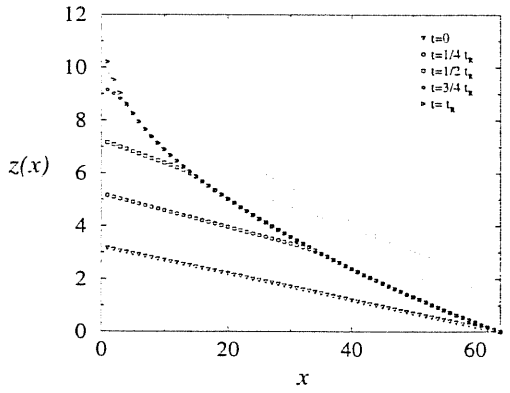

Figure 2.11: Numerical integration of equation (2.14) with a flat plain with slope $-m$ as initial profile, and velocity $-v$ in L (we choose $m = \sqrt{\frac{v}{L}}$). The landscape is shown at three stages of the evolution corresponding to $t = 1/4\,t_R$, $t = 1/2\,t_R$ and $t = 3/4\,t_R$, where $t_R = 2\sqrt{L}/\sqrt{v} - mL/v$ is the value of the relaxing time derived analytically in the previous section. The solid lines correspond to the analytical solution given by eq. (2.23) at the various times.

did not make any assumption).
If we require scaling:

$$z(x,L) = L^{\alpha} f\left(\frac{x}{L}\right) = F(x) - F(L) = F(L)\left(\frac{F(x)}{F(L)} - 1\right), \tag{2.34}$$

then $F(x) = -Ax^{\alpha}$ implying

$$z(x,L) = AL^{\alpha} f\left(\frac{x}{L}\right), \tag{2.35}$$

where $A = z(0,L)$ and $f(s) = 1 - s^{\alpha}$. This is exactly what we found in $d = 1$ with $\alpha = 1/2$ and what we will find (see section 6) for the mainstream in $d = 2$ with the appropriate α.

2.4 Numerical Results in $d = 1$

Equation (2.14) has been solved numerically by direct integration in the simplest case for which the solution is given analytically in order to test the algorithm (results are shown in fig 2.11 with the theoretical predictions). The simulations have been performed then in the case of a random initial condition (fig 2.12) and with an additional diffusive term (fig. 2.13). Moreover the presence of an inhomogeneous rainfall has been considered, and has been found to be irrelevant on the evolution of the profile.
All simulation have been performed on a sample of size 64. In the figures the initial profile and the evolution at four successive times are shown.

In the case of a random initial condition the equation must be generalized in order to be applied to a non-monotone profile. Indeed, in the case of a non monotone profile, the

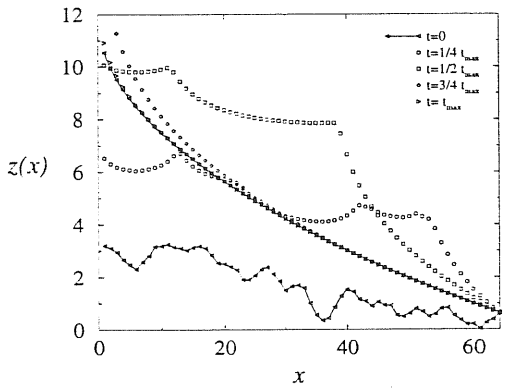

Figure 2.12: As in fig. 2.11 but with a random initial condition.

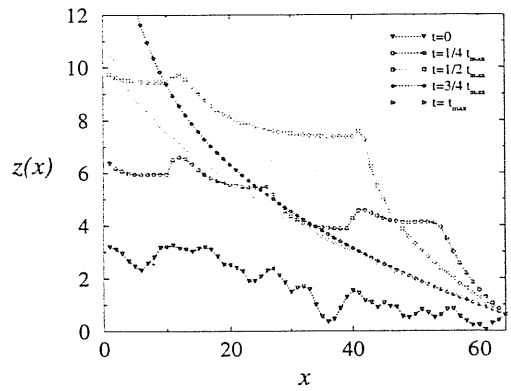

Figure 2.13: As in fig. 2.12 and with the same initial condition of fig 2.12, but with the addition of a diffusive term in the equation.

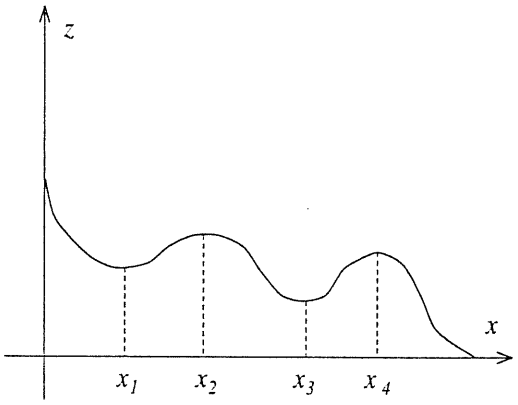

Figure 2.14: Example of a generic initial condition. The flow J must be taken respectively equal to $x, x_2 - x, x - x_2, x_4 - x, x - x_4$ in each monotonic region.

identification of the flow J with x is no more valid. The equation remain the same in each monotonic subset, with the proper direction for the flux, that now depends also on t. The flux must be taken as in the example of fig 2.14. Solving equation (2.14) without the diffusive term would lead to singularities in the points x_2, x_4 in fig. 2.14. The discretization, introducing a diffusive effect, eliminates these singularities, as results evident from fig 2.12. Note that in the points of minima the flux must be taken equal to zero.

We can observe that in the case in which no *lakes* are present in the initial condition, they will never be generated from equation (2.14). Indeed, if $\partial_x z_0(x) \leq 0$ for $x \in (0, L)$, then from equations (2.18) and (2.21) it follows that $\partial_x z(x,t) \leq 0$ at any successive time.

2.5 Description of Scaling Laws

In order to provide a general setting for further considerations we review some basic concepts about the finite size scaling approach to the statistical characterization of river networks. Such networks are known to exhibit power law behaviour typical of fractal structures in the distributions of some quantities characterizing their morphology. Let us define such distributions in the simple case of a lattice model which will be used explicitly also in the next sections.

A landscape is described by a scalar field of elevations, where drainage directions are identified by steepest descent, i.e. by the largest local decrease of the elevation field. Excluding the presence of lakes, i.e. assuming that from each point the water can flow to one of the nearest neighbours, a river network can be represented by an oriented spanning graph over a two dimensional lattice of arbitrary size and shape, in which oriented links (one coming out from each site of the lattice) correspond to drainage directions.

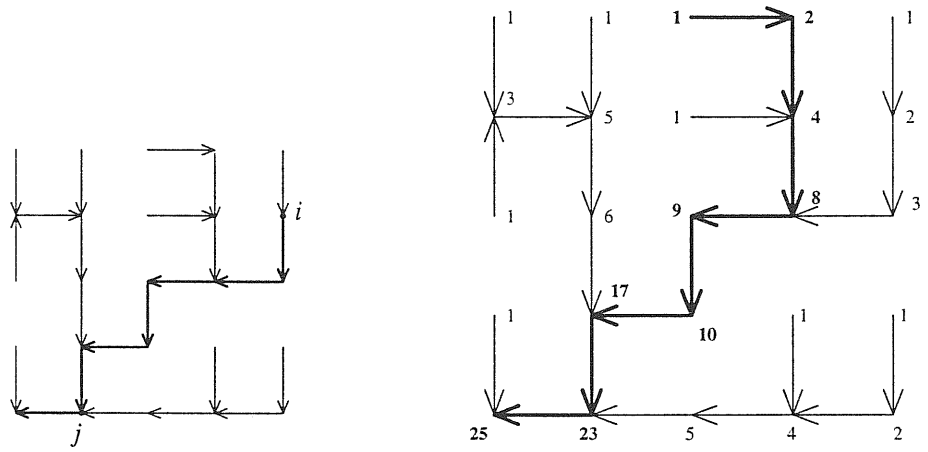

Figure 2.15: Example of drainage network. In the fig. (a) the site i is upstream with respect to the site j. In fig. (b) the numbers correspond to the drained areas and the bold line to the mainstream.

To fix the ideas, consider graphs spanning an $L \times L$ square lattice, with outlets on one edge. We will say that a point i is *upstream* with respect to a point j if there exists an oriented path joining the two points from i to j (see fig. 2.15 a). To each site i of the lattice, we associate a local injection r_i (the average annual rainfall in the site i). The flow J_i, can thus be defined as the sum of the injections over all the points upstream of site i (site i included). In the case of constant injection ($r_i \equiv$ constant) the flux in a point i results to be proportional to the area a_i drained in that point and we will use indifferently this two quantities (see an example in fig. 2.15 b). In natural basins these drained areas can be investigated through data coming from digital elevation maps (DEM's) [19, 20].

By definition, variables J_i are related by the following set of equations:

$$J_i = \sum_j w_{i,j} J_j + r_i \,, \tag{2.36}$$

where $w_{i,j}$ is 1 if site j is a nearest neighbour upstream with respect to site i and 0 otherwise.

Another relevant quantity is the so called upstream length relative to a site, defined as the length of the stream obtained starting from that site and repeatedly moving along the network in the upstream direction towards the nearest-neighbour with biggest area (the one leading to the outlet is excluded, since it is a downstream site), until a source is reached i.e. a site with no incoming links. If two or more equal areas are encountered, one is randomly selected[2].

For a given graph on a lattice of given linear size L we will consider the following two prob-

[2]This is the the operative definition used by geomorphologists to extract the upstream lengths from DEM. It is slightly different to the one we gave in section 2.1 but it should be clear that the difference is irrelevant in a statistical sense, i.e. if we are interested in probability distributions.

ability distributions originally introduced to describe real river basins and experimentally found to scale as power laws:

- $p(a, L)$, the probability density of drained areas a, and
- $\pi(l, L)$, the probability density of the upstream lengths l.

These represent the fraction of sites draining an area a or having an upstream length l respectively. We will also consider the corresponding integrated probability distributions $P(a, L)$, and $\Pi(l, L)$. For such distributions a finite size scaling ansatz has been formulated [10] that seems to provide a simple and natural explanation to well known empirical laws. The finite size scaling ansatz consists in postulating the following form for the distributions:

$$p(a, L) = a^{-\tau} f\left(\frac{a}{a_C}\right), \tag{2.37}$$

$$\pi(l, L) = l^{-\psi} g\left(\frac{l}{l_C}\right), \tag{2.38}$$

where f and g are scaling functions accounting for finite size effects and a_C and l_C are the characteristic area and length respectively which depend on L. The functions f and g are assumed to have the following properties: when $x \to \infty$ they go to zero sufficiently fast to ensure normalization; when $x \to 0$ they tend to a constant, to yield simple power law behaviour of the probability distributions in the large size limit. This also implies that τ and ψ are bigger than one.

The characteristic area and length are assumed to scale as

$$a_C \sim L^{1+H}, \tag{2.39}$$

$$l_C \sim L^{d_f}. \tag{2.40}$$

H is known as the Hurst exponent and is of course $0 \leq H \leq 1$. The d_f exponent, characterizing the typical length, has the meaning of fractal dimension of a stream (each rivulet going from any site to the outlet is assumed to have the same fractal dimension), and is such that $1 \leq d_f \leq 1 + H$.
$d_f = 1$ corresponds to a straight line whereas $d_f = 1 + H$ corresponds to have an almost single space filling rivulet.

The integrated probability distributions can be written as

$$P(a, L) = a^{1-\tau} F\left(\frac{a}{L^{1+H}}\right), \tag{2.41}$$

$$\Pi(l, L) = l^{1-\psi} G\left(\frac{l}{L^{d_f}}\right), \tag{2.42}$$

which follow from (2.37) and (2.38) with

$$F(x) = x^{\tau-1} \int_x^{+\infty} dy\ y^{-\tau} f(y)\,, \tag{2.43}$$

$$G(x) = x^{\psi-1} \int_x^{+\infty} dy\ y^{-\psi} g(y)\,. \tag{2.44}$$

The four exponents introduced up to now are not independent. In fact they have been shown [17] to be related by the following scaling laws[3]:

$$\tau = 2 - \frac{d_f}{1+H}\,, \tag{2.45}$$

$$\psi = \frac{1+H}{d_f}\,. \tag{2.46}$$

The observed values of τ and ψ are in the ranges $1.42 - 1.46$, $1.73 - 1.85$ respectively.

A well known hydrological law, Hack's law [22], relates the length of the longest stream l in the drainage region to the drainage area of the basin a:

$$l \sim a^h\,. \tag{2.47}$$

The accepted values of h range in the interval $h = 0.56 \pm 0.02$ [27, 28, 29]. Their definite departure from the Euclidean value 0.5 lead to the first suggestion of the fractal nature of rivers [23].

From equations (2.39) and (2.40) it follows that

$$h = \frac{d_f}{1+H}\,. \tag{2.48}$$

The scaling relations (2.45) and (2.46) can be expressed in a simpler form, observing that both τ and ψ depend on d_f and H only in the combination $\frac{d_f}{(1+H)} = h$, where h is the

[3] These scaling relations derive from two considerations: the first is the fact that the cumulated areas, averaged over all the sites is equal to the distance from the outlet, averaged over all the sites $\langle a \rangle = \langle l_{downstream} \rangle$. This gives

$$(2-\tau)(1+H) = d_f\,,$$

that is equation (2.45).
The other is the fact that Hack's law suggests the existence of a well defined constraint between lengths and areas, implying that conditional probability $\tilde{\pi}(l \mid a)$ of finding a main stream with length l in a basin draining an area a is a sharply peaked function of l: $\tilde{\pi}(l \mid a) = \delta(l - a^h)$ or more generally $\tilde{\pi}(l \mid a) = l^{-1}\tilde{g}(\frac{l}{a^h})$.
π, p and $\tilde{\pi}$ must be related by a consistency equation:

$$\pi(l, L) = \int_1^{L^{1+H}} \tilde{\pi}(l \mid a) p(a, L) da\,,$$

that,in the large L limit, gives

$$(\psi - 1) df = (\tau - 1)(1+H)\,.$$

From this relation and (2.45), (2.46) follows.

parameter appearing in Hack's law (2.47). Thus

$$\tau = 2 - h, \tag{2.49}$$

$$\psi = \frac{1}{h}. \tag{2.50}$$

The exponents τ and ψ are thus related by the simple expression:

$$\tau = 2 - \frac{1}{\psi}. \tag{2.51}$$

Since $1 \leq d_f \leq 1 + H$ and $H \leq 1$ it follows that $1/2 \leq h \leq 1$. This implies that $\tau \leq 3/2$. The equality holds only when $H = d_f = 1$ which corresponds to the mean field situation [17, 14].

2.6 2-dimensional River Networks

In this section we report our results on the analysis of equation (2.4) in $d = 2$, corresponding to the physical case. These results come from computer simulations joined with some analytical arguments.

In subsection 6.1 we describe an iterative algorithm for the search of stationary solutions of equation (2.4).
All data regarding the stationary solutions have been obtained with this method. They are analyzed in detail in subsections 6.2 and 6.3.
In particular, in subsection 6.2 we analyze the distributions of drained areas and mainstream lengths, and in section 6.3 the scaling properties of the "average" profile and of the profile along the mainstream. The profile along the mainstream is deduced also from analytical arguments, thanks to the fact that it is topologically one dimensional.
The iterative algorithm turns out to be much faster than a direct integration of the equation and thus reveals to be very useful to get richer statistics. However it does not give informations about dynamic itself, i.e. about the behaviour of the system during the evolution, in particular if one is interested on the disappearance of lakes and on relaxation times.
For this reason a numerical study with standard methods has also been performed. Results are reported in subsection 6.4 .

All simulations described in this section refer to a square lattice with periodic boundary conditions on one direction and open boundary conditions on the other one.

2.6.1 Description of The Iterative Algorithm

We are looking for stationary solutions of equation (2.4). Any stationary solution must satisfy

$$\alpha J \mid \nabla z \mid^2 = v\,, \tag{2.52}$$

where v is a constant velocity imposed by the boundary conditions[4] on the lower edge. Thus for a stationary solution, the relation

$$\mid \nabla z \mid = \sqrt{\frac{v}{\alpha}} J^{-\frac{1}{2}} \tag{2.53}$$

between flux and gradient must hold in any point.

The landscape is described giving a field of elevations $\{z_i\}$. The drainage basin can be reconstructed using the rule of the *steepest descent* i.e. assuming that the flux in a point has the direction of the maximum gradient of the elevation field (the direction of the lowest of all nearest neighbours). This is correct as far as there are not *lakes*. We will call *compatible* a field of elevations that satisfy this request. Since our equation has been shown numerically in $d = 1$ to eliminate lakes during the evolution and have been proved not to form them again, we restrict ourselves for simplicity to landscapes described by compatible fields of elevations. It is then clear that to any of such landscapes one can uniquely associate an oriented spanning graph on the lattice, i.e. an oriented graph loopless and passing through each point. Now, identifying the flux in a point with the total area drained in that point, one can reconstruct the field of fluxes $\{J_i\}$ corresponding to a given oriented spanning graph. The flux in a site is simply given by the number of sites upstream with respect to that site in the case of uniform rainfall, and is given by equation (2.36) in the more general case. From the fluxes a new field of elevations can be defined using equation (2.53). The new configuration of the landscape will be again compatible since each point has at least one nearest neighbour with biggest flux, that is the one in which it flows, and then from (2.53) it has at least one nearest neighbour with smaller height.

We can thus define a transformation from the set of compatible configurations in itself:

$$\{z'_i\} = \mathcal{T}(\{z_i\}) \tag{2.54}$$

consisting in the following chain of transformations:

$$\{z_i\} \xrightarrow[\text{steepest descent}]{} \underset{\text{graph}}{\text{spanning}} \xrightarrow[\text{drained areas}]{} \{J_i\} \xrightarrow[\text{equation 2.53}]{} \{z'_i\}$$

Any fixed point of equation (2.54) is a stationary solution of equation (2.4).

[4] As noted in subsection 2.3, the presence of an uplift term $\neq 0$ is of crucial importance. An uplift equal 0 would cause the complete flattening of the surface. This is indeed what happens in ref. [7]. .

2.6.2 Scaling of Drained Areas and Upstream Lengths

We performed simulations on samples of different sizes starting, for each size, with 100 different initial conditions.

We started the algorithm giving a spanning graph as initial condition. The initial networks have been constructed in the following way: we chose a site at random and let it follow a random walk until it reach a site on the edge containing the outlets. Then another site is randomly selected among the ones not visited by the previous walks and a new random walk is generated till it visits one site on the edge containing the outlets or it intersects the already existent pattern (consisting in the union of the previous random walk(s) but the present). If, before to do that, this walk intersects itself in some point i, the oldest of the two links outcoming from i is deleted in order to eliminate the loop.
All this procedure is repeated until all sites have been touched. The distributions (2.41) and (2.42) of such spanning graphs has been tested in order to check to which universality class (assumed to be identified by the exponents in the power laws introduced in section 5), they belong to. We found $\tau = 0.40 \pm 0.03$ and $\psi = 0.67 \pm 0.03$.

For sizes 32, 64, 128 and 256, starting from configurations generated in this way and iterating the algorithm described in subsection 6.1 we got stationary solutions of equation (2.4).
The distributions of drained areas and mainstream lengths show power law behaviour. The exponents are nearly the same for each configuration and are different from the ones we started from.
Averages over the 100 stationary solutions give for the exponents respectively $\tau = 1.45 \pm 0.02$ and $\psi = 1.82 \pm 0.02$. Log-log plots of these integrated probability distributions of cumulated areas and upstream lengths are shown respectively in fig. 2.16–2.17 and fig. 2.19–2.17.

Collapse test have been done in order to evaluate the exponents defining the characteristic area and length that result to be: $1+H = 1.98 \pm 0.04$, $d_f = 1.10 \pm 0.04$. Collapses are shown in fig. 2.18 and 2.21. These numerical values are in perfect agreement with the scaling laws in section 5.

To have a direct measure of the exponent h appearing in the Hack law, we plotted the drained areas along the mainstream against the corresponding upstream length (see the inset in fig. 2.26, in the next subsection). We found a good power law with an exponent $h = 0.55 \pm 0.02$ in good agreement both with the values of H and d_f and with the value observed in Nature.

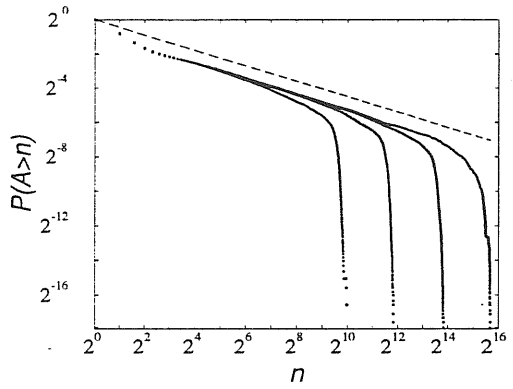

Figure 2.16: Integrated probability distribution of cumulated areas averaged over 100 samples on 32×32, 64×64, 128×128 and 256×256 square lattices. The slope of the dashed line is $\tau - 1 = 0.45$.

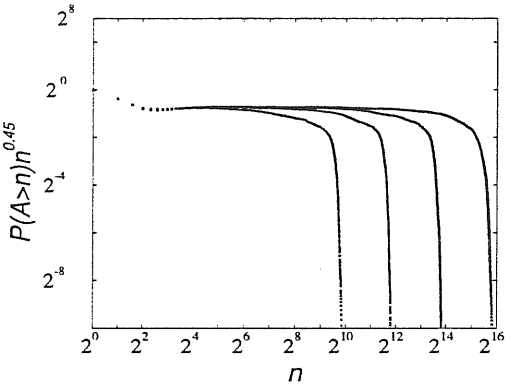

Figure 2.17: Integrated probability distribution of cumulated areas times $n^{0.45}$ averaged over 100 samples as in fig. 2.16.

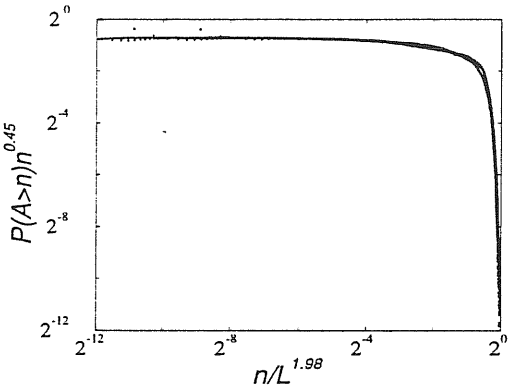

Figure 2.18: Collapse plot for the distributions of fig. 2.16 obtained with $\tau = 1.45$ and $1 + H = 1.98$.

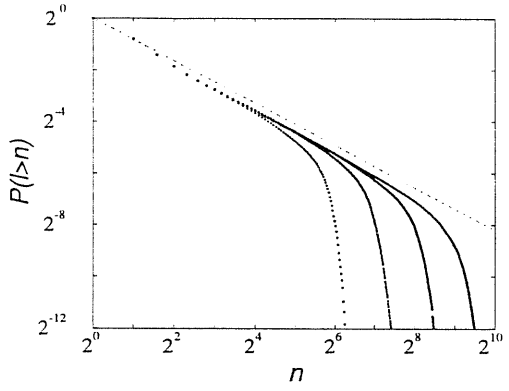

Figure 2.19: Integrated probability distribution of mainstream lengths averaged over 100 samples on 32×32, 64×64, 128×128 and 256×256 square lattices. The slope of the dashed line is $\psi - 1 = 0.82$.

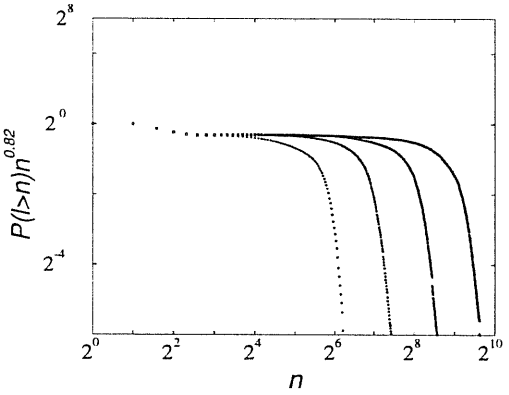

Figure 2.20: Integrated probability distribution of mainstream lengths times $n^{0.82}$ averaged over 100 samples as in fig. 2.19.

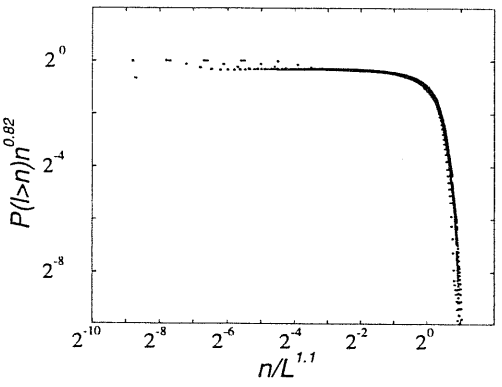

Figure 2.21: Collapse plot for the distributions of fig. 2.19 obtained with $\psi = 1.82$ and $d_f = 1.1$.

2.6.3 Scaling of Profiles and Profile along the Mainstream

Let x be the direction parallel to the edge containing the outlets in the "substrate" plane, i. e. the edge which is lowering with velocity v, and y the one perpendicular. For each sample we considered the one dimensional profiles obtained taking slices in the x direction at constant y and considering for each value of y the mean height and the corresponding roughness (see fig. 2.22).

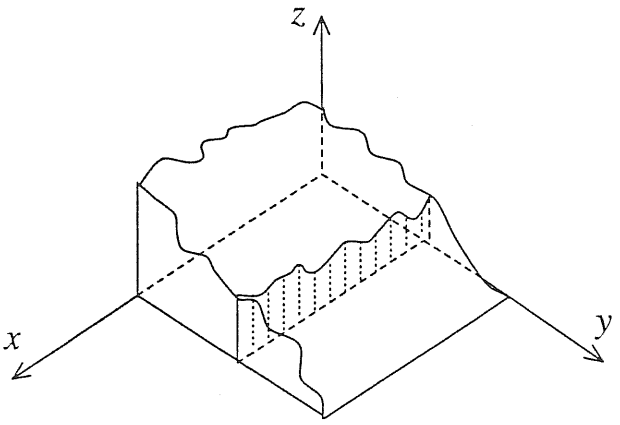

Figure 2.22: Slices for the average profile.

Profiles and roughness averaged over all x show again scaling properties. The height of the profile is found to have the form:

$$z(y) = L^{\alpha} f_z\left(\frac{y}{L}\right) \tag{2.55}$$

with a numerical value for the exponent of $\alpha = 0.20 \pm .05$ (see fig. 2.23 (a), 2.24). Likewise for the roughness in the $y = const$ plane

$$w(y) = L^{\gamma} f_w\left(\frac{y}{L}\right) \tag{2.56}$$

with $\gamma = 0.20 \pm 0.05$ (see fig. 2.23 (b), 2.24).

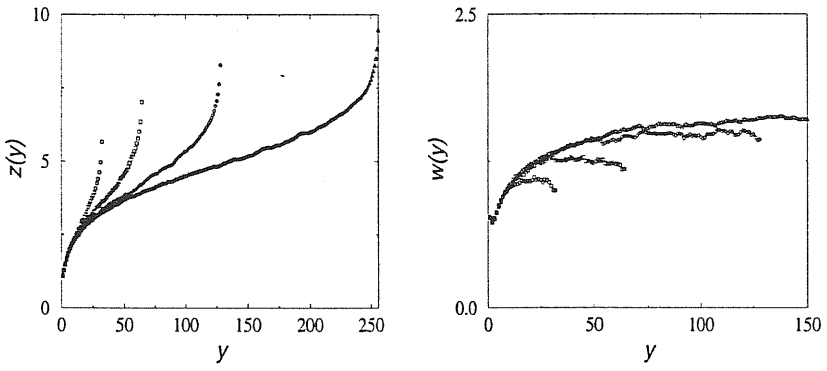

Figure 2.23: Averaged profiles (a) and roughness (b) along the x direction plotted versus y for sizes 32, 64, 128 and 256.

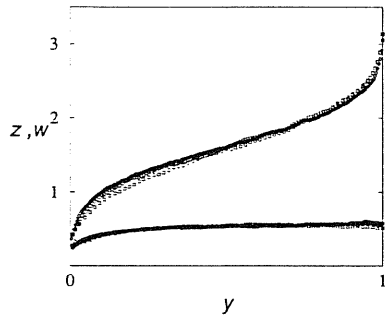

Figure 2.24: Reasonable collapses of averaged profiles and roughness are obtained with $\alpha = .2$ and $\gamma = .2$.

Moreover we reconstructed the profile along the mainstream.
This have again scaling properties with a law analogous to that of the averaged profiles (2.55) were L is replaced with the length of the mainstream $\mathcal{L}$ and with a different value $\tilde{\alpha}$ of the exponent:

$$z(l) = \mathcal{L}^{\tilde{\alpha}} \tilde{f}_z\left(\frac{l}{\mathcal{L}}\right). \tag{2.57}$$

In (2.57) l refers to the length along the stream and $\mathcal{L}$ represents the mainstream length. The value of $\tilde{\alpha}$ is $\tilde{\alpha} = 0.09 \pm 0.01$ definitely smaller than the value of α in (2.55).
This is not surprising since by definition, going back up along the main stream, at each step one chose the direction of the site with biggest area, i.e. for the relation (2.53), the direction of the smallest gradient. The resulting path is then systematically lower than a generic one.

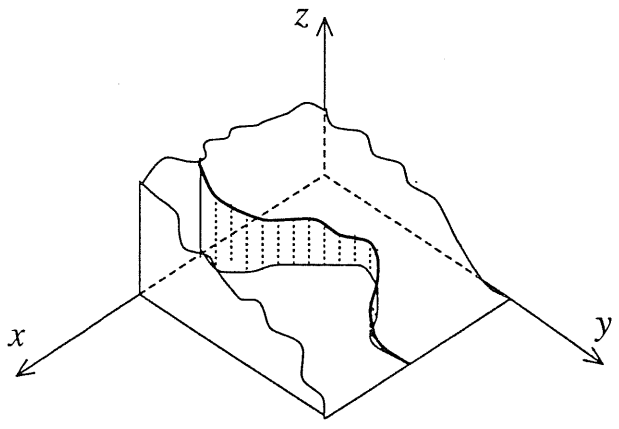

Figure 2.25: Profile along the mainstream.

It is very interesting to note that equation (2.57) can be recovered analytically with the correct exponent and with the explicit form of the scaling function with the following argument: the evolution along the mainstream can be regarded as an effective one dimensional problem if one take properly into account the fluxes along the stream. Thus we argue that the behaviour of $z(l,t)$ is well described by equation (2.14) replacing x in the right hand side with l^{ν}. The value of ν is expected to be given by the exponent $h^{-1} = \frac{1+H}{d_f}$ relating the area drained in a point with the upstream length relative to that point (see equation (2.47)).

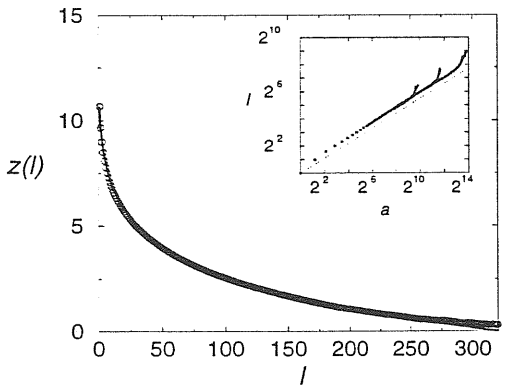

Figure 2.26: Profiles along the mainstream obtained in two dimensional simulations on a 128×128 square lattice and averaged over 100 samples starting from different randomly chosen initial conditions. The solid line is the analytical result in dimension one with an exponent $h = 0.55$. The value of h has been obtained from the log-log plot of the upstream lengths along the mainstream versus the corresponding areas shown in the inset. Numerical values and theoretical prediction are practically indistinguishable.

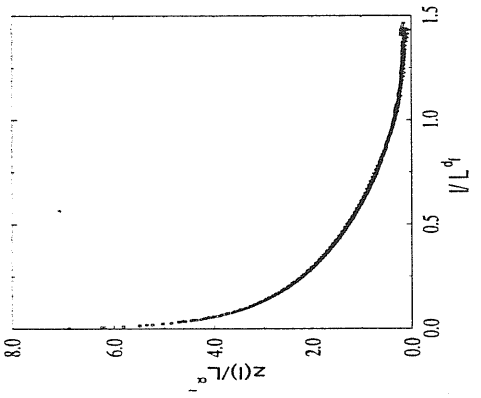

Figure 2.27: Collapse of profiles along the mainstream corresponding to 32×32, 64×64, 128×128 and 256×256 square lattices obtained with $\tilde{\alpha} = 0.09$ and $d_f = 1.1$.

Thus we are lead to the following equation for the main stream evolution (after the imprinting of the drainage directions has occurred (sec. 2.4.6))

$$z_t(x,t) = -kx^\nu z_x^2(x,t) \tag{2.58}$$

with initial conditions

$$\begin{cases} z(x,0) = z_0(x) \\ \partial_t z(\tilde{L},t) = -v\,. \end{cases} \tag{2.59}$$

This can be solved with the same method used in section 3 with the substitution $y = x^{1-\frac{\nu}{2}}$ unless $\nu = 2$. The stationary solution is given by

$$z(x,t) = \frac{1}{\mu}\sqrt{\frac{v}{k}}(L^\mu - x^\mu) - vt \tag{2.60}$$

where $\mu = 1 - \frac{\nu}{2}$.

Using $\nu = h^{-1} = \frac{1+H}{d_f}$ we get $\mu = 1 - \frac{\nu}{2} = 1 - \frac{1+H}{2d_f} \approx 0.09$. μ corresponds to the scaling exponent $\tilde{\alpha}$ in equation (2.57). The value of $k \approx 0.51$ has been extrapolated from the log-log plot of fig. 2.26 where the cumulated areas along the mainstream are plotted against the upstream length. This analytical expression for z fits surprisingly well with the profiles obtained with the simulations, how is shown in figure 2.26 for the samples of size 128. Figure 2.27 show the collapse of the profiles of sizes 32, 64, 128 and 256.

2.6.4 Relaxation and Freezing Times

A direct integration of the two dimensional equation proves to be slow, and then we are able up to now only to give qualitative results: simulations show that there are two disparate time scales associated with the dynamics. The first of these is the time t_F (*freezing time*) taken to determine the connectivity of the spanning tree and it is relatively fast. This was also observed in [7]. The second, t_R (*relaxing time*) involves further erosion without changing the spanning tree, until the soil height acquires a stable profile that satisfies equation (2.53). This may account for the robustness of the scaling statistics associated with the spanning trees, as the imprinting of the tree occurs relatively early in the evolution process.

2.7 Results in $d = 2$ with Additive Noise

Heating the system with an additive noise term, and carefully quenching, enables to reach more stable solutions, with different statistic.

Simulation described in subsection 6.2 have been repeated starting from 10 initial conditions chosen as in subsection 6.2 for the equation

$$\dot{h}(t,\underline{x}) = -\alpha J(t,\underline{x}) \mid \vec{\nabla} h(t,\underline{x}) \mid^2 + \eta(t,\underline{x})\,. \tag{2.61}$$

where $\eta(t, \underline{x})$ are independent variables identically distributed with uniform distribution with zero mean and variance ($\langle \eta(t^1, \underline{x}^1)\eta(t^2, \underline{x}^2)\rangle = D\delta_{t^1,t^2}\delta_{\underline{x}^1,\underline{x}^2}$).

A brief sketch of the algorithm is as follows:

i) Generation of a random initial configuration:

We generate randomly an initial configuration as described in sec 6.2.

ii) Evolution of the configuration:

The system is evolved with the algorithm described in subsection 6.1 apart for the fact that v in equation (2.53) is replaced by $v+\eta(t, \underline{x})$, for $4 \times L \times L$ iterations.

iii) Lowering of the variance D:

In each cycle the variance D of the noise distribution is lowered by a factor $\alpha' \simeq .95$ by decreasing the interval of definition of η of a factor $\alpha = 0.983$. At the first cycle $\eta \in [-v\alpha, v\alpha]$, at the n^{th} cycle $\eta \in [-v\alpha^n, v\alpha^n]$.

After step *i*), steps *ii*) and *iii*) are repeated many times, till D reaches very low values ($\approx 10^{-4}$). The entire algorithm is repeated from step *i*) with a new initial condition.

The distributions of drained areas and mainstream lengths show power law behaviour with exponents respectively $\tau = 1.50 \pm 0.03$ and $\psi = 1.98 \pm 0.03$, as shown in fig. 2.28 The exponents for the characteristic area and length are found to be $1 + H = 1.98 \pm 0.05$ and $d_f = 1.00 \pm 0.05$ from the collapses. The exponent h has been extrapolated from the log-log plot of drained areas along the mainstream with respect to the corresponding upstream lengths and result to be $h^{-1} = 2.00 \pm 0.05$.

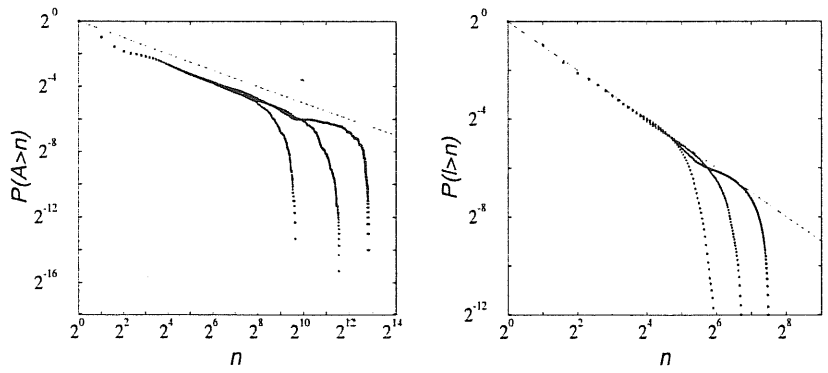

Figure 2.28: Averaged distributions of drained areas (a) and upstream lengths (b) for sizes 32, 64, 128. The solid lines correspond to slopes .5 and 1 respectively.

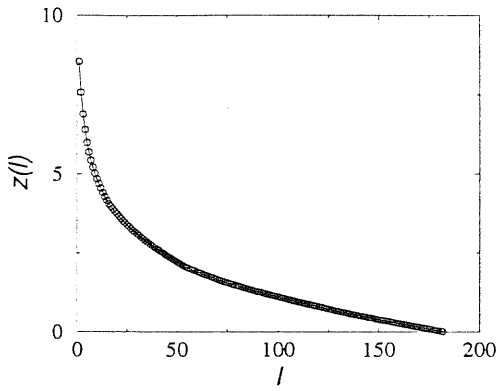

Figure 2.29: Profile along the mainstream for a size 128. The solid line corresponds to the theoretical prediction.

Scaling of the profiles along the mainstream has also been tested. We found a logarithmic behaviour of z with $\mathcal{L}$. This is in perfect agreement with the argument in dimension one: equation (2.58) with $\nu = 2$ cannot be solved with the substitution $y = x^{1-\frac{\nu}{2}}$. Anyway solving equation (2.58) with $\nu = 2 - \varepsilon$ and taking the limit $\varepsilon \to 0$ in the solution one gets

$$z(x,t) = -\sqrt{\frac{v}{k}} \log\left(\frac{L}{x}\right) - vt \tag{2.62}$$

that solves equation (2.58) with $\nu = 2$.
In fig. 2.29 the profiles obtained by simulation for a size 128 are compared with the theoretical prediction. The value of k, as in section 6.2 has been extrapolated from the log-log plot of the areas along the mainstream versus the corresponding upstream length.
Note that a naive scaling argument as in section 2.3 gives again the correct result: assuming the scaling of x, z and t with L

$$x \sim L \quad , z \sim L^{\alpha} \quad , t \sim L^{\zeta}, \tag{2.63}$$

and observing that the noise term scales as $(x^{-1}t^{-1})^{1/2} \sim L^{-\frac{1+\zeta}{2}}$, one gets

$$\begin{cases} \alpha - \zeta = 2\alpha - 1 \\ \alpha - \zeta = -\frac{1+\zeta}{2} \end{cases} \tag{2.64}$$

that gives $\zeta = 1$ and $\alpha = 0$, in accordance with the logarithmic behaviour found in (2.62). Also in this case, the possible diffusive terms seems irrelevant since it should scale as $L^{\alpha-2}$.

2.8 Results in $d = 2$ with Random Injection

Natural river basins are known to be heterogeneous. The simplest heterogeneity that one may consider is random precipitation with r_i no longer being uniform. Sites with large

drained area have contributions from the r_i of all the upstream sites. Thus, fluctuations in r_i that do not have a long tail in their distribution would be expected to average out to yield the homogeneous result. Indeed a numerical study of this case shows that, as in $d = 1$, the universality class is unchanged on adding this kind of heterogeneity.

2.9 Discussion, conclusions and outlook

The model proposed and analyzed in this chapter seems in spite of its simplicity to capture lot of features of landscapes evolution. The evolution equation is derived from very general considerations and provide a good qualitative and quantitative explanation for all the observed facts: the Hack's law, the slope-discharge relation, the power law distributions of drained areas and upstream lengths. It also predict the exact scaling of two quantities, the average profile and the profile along the mainstream that may be deduced from observational data and would provide a good test of our theory.

There is one point that is still unclear and is the fact that as a consequence of short freezing times corresponding to a very rapid imprinting of the landscape, the final drainage configuration of the network has a strong dependence on the initial condition. This can account for the range of values observed for τ and ψ but opens the question of what is a good physical choice for the initial configuration. Note however that this problem does not affect at all our result on the evolution of the profile and the relative scalings.

Another interesting question is to clarify if networks resulting from this erosional dynamics are related to the configurations (Optimal Channel Networks (OCN) [15, 16]) arising from the minimization of the total dissipated energy. Addressing this question will be part of the subject of the next chapter.

3 Optimization and branching patterns

Lot of branching patterns are observable in Nature . Some beautiful examples are shown in the first chapter (fig 1.1, 1.2 and 1.3).

Starting from a river network model and generalizing to any open dissipative system with injection we show that branching structures may arise from optimization of a cost function with the constraint that the continuity equation be satisfied.

In this chapter (section 1) we introduce the *Optimal Channel Network* (OCN) model for river networks, based on a principle of minimum dissipated energy expenditure. Minimum energy dissipation rate models are based on the postulation that an open system with constant injection evolves toward a structure that minimizes the total energy dissipation rate.
Drainage basins, subject to a uniform energy input from precipitation are an example of this type of systems and they may form a structure that minimizes the rate of energy dissipation in the whole basin.

For the OCN model the statistical features of the global minimum are exactly known. Local minima are statistically indistinguishable from configurations observed in Nature and quite different from the global solution. This consideration suggested the concept of *feasible optimality* [30] (the discussion of which is postponed to section 5) claiming that Nature is unable to reach the true ground state in complex optimization problems and that local minima, having well defined statistical properties belong to a new universality class.
Some evidences of that comes also from the study of domain walls in random ferromagnets.

Optimal configurations coming from the OCN model are shown (section 2) to be stationary solutions of the equation describing landscapes evolution analyzed in the previous chapter, in the sense that the landscape reconstructed from an optimal drainage network with the slope-discharge rule is consistent with the fact that the flow follows the steepest descent. This is not at all a trivial fact.

Another system which is known to arrange itself in order to minimize the rate of energy

dissipation is a resistor network (section 3). The key difference is that in a network of resistors there is just one configuration minimizing the total energy dissipation, while in the river network case the energy landscape has been found to be riddled with a lot of local minima.

In section 4 we show how loopless structures may arise as optimal structures minimizing a cost function with the constraints imposed by the continuity equations.
In the river networks case, if one enlarge the configurations space allowing configurations in which the flow can split in more directions (i.e. renouncing to the statement that the all flow run in the direction of the steepest descent), and minimizes the dissipated energy, one recovers the spanning loopless configurations. Thus loopless trees are minima of the dissipated energy with respect to small variations of the flow.

3.1 Optimal Channels Network Model

To each landscape $\{z_i\}$ defined on a lattice as in section 2.1 we associate a dissipation energy as

$$E = \sum_i k_i J_i \Delta z(i) \tag{3.1}$$

where $\Delta z(i)$ is the height drop along the drainage direction, J_i is the flow through the site i. and k_i is a quantity related to the soil properties such as erodability, vegetation, lithology etc. For homogeneous basins $k_i = 1$ without loss of generality.

Field investigations [31, 32, 33] shown that the velocity of the flow tends to be constant throughout the network. Thus the energy dissipated to maintain the water flow, equals the potential energy associated with precipitation. The power dissipation in a link is $J_i \Delta z_i$ and then the (3.1) represents the power expenditure in the whole system.

Using the empirical law $\Delta z(i) \sim J_i^{0.5}$ [34. 31, 35] equation (3.1) can be rewritten as

$$E(T) = \sum_i J_i^{\gamma} . \tag{3.2}$$

where $\gamma = 0.5$ and T represents the oriented spanning graph associated to the landscape. The Optimal Channels Networks [15, 16] consist of the configurations T which are local minima of the dissipated energy (3.2) in the sense specified below:
we will say that two configurations T and T' are *close* if one can go from one to the other just changing the direction of one link, i.e. if the set of links $T \cup T'$ represent a graph with a single loop (see fig 3.1). A configuration T is said a local minimum of the functional (3.2) if to each *close* configuration T' corresponds a bigger energy. Note that not all changes are allowed in the sense that the new graph needs again to be loopless.
Thus a local minima is a stable configuration under a "single link flip $T = 0$ dynamic", i.

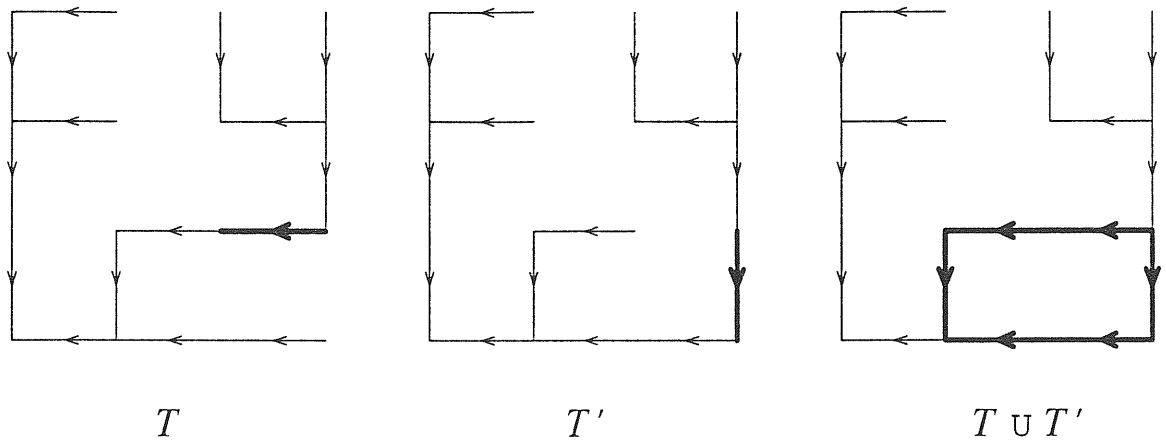

Figure 3.1: Example of two *close* configurations.

e. a dynamic in which only one link at times can be flipped, and it is flipped only when the move does not creates loops and decreases the functional (3.2).

Numerical analysis on this OCN model [14] lead to the conclusion that the energy landscape is riddled with a large number of local minima characterized by similar values of $E(T)$. As "statistical indicators" one can choose the exponents in the probability distributions of cumulated areas $P(a > n) \propto n^{-(1-\tau)}$ and of upstream lengths $P(l > n) \propto n^{-(1-\psi)}$ (see section 2.5), that for real rivers gives the experimental values $1 - \tau = 0.44 \pm 0.02$ and $1 - \psi = 0.79 \pm 0.06$.
Interestingly, OCN's show features in remarkable agreement with real data only when "imperfect"searching procedures (like this $T = 0$ dynamic) are used. For the global minimum, the exact value of the exponents are known [14, 17] and are $1 - \tau = 1/2$ and $1 - \psi = 1$, significantly different from the ones of local minima.
This has been the starting point for the formulation of the concept of feasible optimality [30], that we will briefly discuss in the last section.

3.2 Relation with the Model of Landscape Evolution

We will prove that any elevation field corresponding through the relation

$$| \vec{\nabla} z_i | \sim J_i^{1/2} \tag{3.3}$$

to a configuration minimizing at least locally the functional of equation (3.2) is a stationary solution of equation:

$$\dot{z}(t, \underline{x}) = -J(t, \underline{x}) \, | \, \vec{\nabla} z(t, \underline{x}) \, |^2 \ . \tag{3.4}$$

The proof is as follows: consider a configuration realizing a local minimum of the dissipated energy, and a site i. The link outcoming from i will go in one of the nearest neighbours

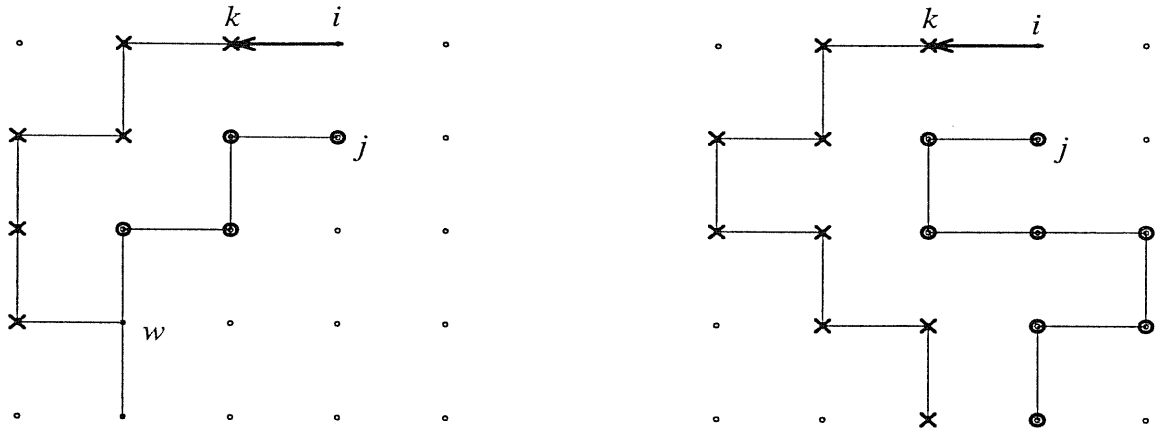

case (a) *case (b)*

Figure 3.2: Example of the two cases (a) and (b). Sites belonging to S_{k_j} are denoted with crosses, sites belonging to S_{j_k} are denoted with circles.

of i, let us say k. Let j be one of the other nearest neighbours such that changing the link from $i \rightarrow k$ to $i \rightarrow j$ one still gets an allowed configuration. Paths outcoming from k and j will intersect downstream in a given point w (case a) or will never intersect until they reach their outlets (case b). Let S_{k_j} denotes the set of all points in the path from k to w in the first case and from k to its outlet in the second (see fig. 3.2). Likewise for j.

Changing the link from $i \rightarrow k$ to $i \rightarrow j$ only the areas of sites belonging to the sets S_{k_j} and S_{j_k} will change. In particular all areas in the set S_{j_k} will be increased of an amount equal to the area $a(i)$ contributing to the flow through i, and all areas in the set S_{k_j} will be decreased of that amount. Thus such a change will cause a change ΔE in the dissipated energy equal to

$$\Delta E = \sum_{x \in S_{j_k}} [(a(x) + a(i))^\gamma - a(x)^\gamma] + \sum_{x \in S_{k_j}} [(a(x) - a(i))^\gamma - a(x)^\gamma], \tag{3.5}$$

where $\gamma = 1/2$ and $a(x)$ are the the fluxes before the flip.

The condition for a configuration to be a local minimum of E translates in the set of conditions

$$\sum_{x \in S_{j_k}} [(a(x) + a(i))^\gamma - a(x)^\gamma] + \sum_{x \in S_{k_j}} [(a(x) - a(i))^\gamma - a(x)^\gamma] > 0 \tag{3.6}$$

for each i and j such that j is a nearest neighbour of i and gives rise to a loopless configuration.

Our aim is to show that conditions (3.6) imply that the elevations field determined by the local minimum configuration using (3.3) represent a stationary solution of equation (3.4).

To that purpose it will be useful to express the condition of stationarity in a more explicit form. In order to be a stationary solution of equation 3.4 the elevations field determined by a graph trough (3.3) must be such that reconstructing from it the draining directions with the steepest descent rule, one gets back again the graph from which the elevations field originated from. This would imply that if $i \rightarrow k$ is the drainage direction in the point i, the biggest drop in elevation from i to its nearest neighbours is in the direction of k. Then this condition reads:

$$z(k) < z(j) \tag{3.7}$$

for any j nearest neighbour of i and different from k. In the same notations of equations (3.5, 3.6), the height in this two point can be written as:

$$\begin{aligned} z(k) &= z(w) + \textstyle\sum_{x \in S_{j_k}} a(x)^{-\frac{1}{2}} \\ z(j) &= z(w) + \textstyle\sum_{x \in S_{k_j}} a(x)^{-\frac{1}{2}} \end{aligned} \tag{3.8}$$

in the case a and

$$\begin{aligned} z(k) &= \textstyle\sum_{x \in S_{j_k}} a(x)^{-\frac{1}{2}} \\ z(j) &= \textstyle\sum_{x \in S_{k_j}} a(x)^{-\frac{1}{2}} \end{aligned} \tag{3.9}$$

in the case b (the outlets are at zero height being the constant drift subtracted). In both cases inequality (3.7) becomes

$$\sum_{x \in S_{j_k}} a(x)^{-\frac{1}{2}} < \sum_{x \in S_{k_j}} a(x)^{-\frac{1}{2}} . \tag{3.10}$$

In order to proof that eq (3.6) implies equation (3.10), let us observe that eq (3.6) can be rewritten as:

$$\sum_{x \in S_{j_k}} \gamma \int_{a(x)}^{a(x)+a(i)} y^{\gamma-1} dy > \sum_{x \in S_{k_j}} \gamma \int_{a(x)-a(i)}^{a(x)} y^{\gamma-1} dy . \tag{3.11}$$

Since $\gamma < 1$ the integral on the l.h.s. of equation (3.11) is lower than $a(x)^{1-\gamma} a_i$ and the one on the r.h.s. is bigger than $a(x)^{1-\gamma} a_i$. Thus equation (3.11) implies

$$\sum_{x \in S_{j_k}} a(x)^{\gamma-1} > \sum_{x \in S_{k_j}} a(x)^{\gamma-1} \tag{3.12}$$

and then equation (3.10) follows since $\gamma = 1/2$.
The proof holds in the more general case of $0 < \gamma < 1$ and equation (3.3) is substituted with $\mid \vec{\nabla} z \mid \propto J^{1-\gamma}$.

Under this kind of perturbations, the converse is not true, i.e. a stationary solution of equation (3.4) not necessarily realizes a local minimum of the dissipated energy (under this dynamics). Counterexamples can be easily constructed. For example, configurations in which occurs the situation shown in fig. 3.3 are stationary solutions of equation (3.4) for any $a_1 \leq a_2 + q$ while they are <u>not</u> local minima of (3.4) as soon as $a_2 < a_1$. Thus, for any

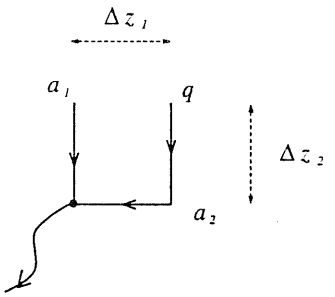

Figure 3.3: One possible counterexample. A stationary solution of equation (3.4) not necessarily realizes a minimum of 3.1. Indeed, in the case in the figure stationary solution $\Rightarrow$ $\Delta z_2 \leq \Delta z_1 \Rightarrow (a_2+q)^{-1/2} \leq a_1^{-1/2} \Leftrightarrow a_1 \leq a_2 + q$; not a local minimum of the energy $\Leftarrow$ $(a_2+q)^{1/2} + a_1^{-1/2} > a_2^{-1/2} + (a_1+q)^{1/2} \Leftrightarrow (a_1+q)^{1/2} - a_1^{-1/2} < (a_2+q)^{1/2} - a_2^{-1/2} \Leftrightarrow a_2 < a_1$.

choice of a_1, a_2 and q such that $a_2 < a_1 \leq a_2 + q$ this provides a counterexample.
Maybe there exists a restricted set of perturbations under which that the converse holds, but this problem is still open.

3.3 An Example of Dissipative System: Resistor Networks

In electrical networks the currents arrange themselves in order to minimize the total dissipated energy. In this case, the dissipated energy is

$$E_D = \frac{1}{2} \sum_{i,j} R_{ij} I_{ij}^2 \tag{3.13}$$

where R_{ij} and I_{ij} are respectively the resistance of the link from i to j and the current flowing through it and $I_{ji} = -I_{ij}$. A continuity equation ensuring the conservation of charge can be written for each site j. Let us call A the point in which the current (for example equal to one) is injected and B the point through which current flows out. Then the continuity equations are

$$\sum_i I_{ij} = \delta_{j,A} - \delta_{j,B} \tag{3.14}$$

(one can as well do the more general case where each site j exchanges a current J_j -positive or negative- with the exterior, with $\sum_j J_j = 0$).
Using Lagrangian multipliers one can minimize the energy (3.13) with the constraints (3.14) and gets

$$\lambda_i - \lambda_j = I_{ij} R_{ij} \tag{3.15}$$

Thus, identifying λ_j with the potential V_j at the point j one recovers the Ohm's law.

One can show that any other currents configuration gives a bigger value of the energy [36]: any other currents configuration I'_{ij} must as well satisfy the constraints (3.14). Let us

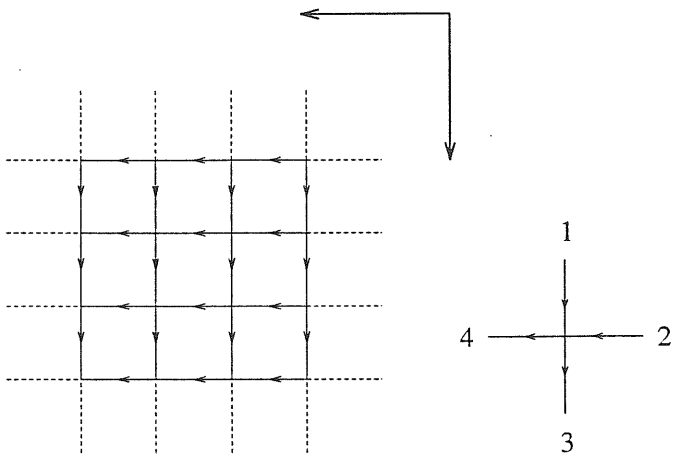

Figure 3.4: Portion of a lattice showing the orientation of bonds.

write $I'_{ij} = I_{ij} - p_{ij}$ ($p_{ji} = -p_{ij}$), then $\sum_{i,j} p_{ij} = 0$. The difference between the energy in the two configurations is $E' - E = \frac{1}{2}\sum_{ij} R_{ij}(-2I_{ij}p_{ij} + p_{ij}^2)$. Observing that the constraints on $\{p_{ij}\}$ imply $\sum_{i,j} R_{ij}I_{ij}p_{ij} = \sum_{i,j}(\lambda_i - \lambda_j)p_{ij} = -2\sum_{i,j}\lambda_i p_{ij} = 0$, one gets $E' > E$.

3.4 Minimum Energy and Loopless Structures

3.4.1 Equations for the currents

Consider a square lattice. Fix an orientation for all lattice bonds (e.g. the ones of the positive axis as in fig 3.4). On each bond b a current i_b is defined. $i_b > 0$ if it is flowing in the assigned direction, $i_b < 0$ otherwise. Uniform (unitary) injection (rainfall in the case of river networks) is equivalent to the set of constraint

$$(\partial i)_x = 1 \tag{3.16}$$

where ∂ is a sort of discrete version of the divergence (see fig 3.4 for the notations):

$$(\partial i)_x = -i_1 - i_2 + i_3 + i_4 \tag{3.17}$$

We want to show that a local minima of the cost function

$$E = \sum_b |\, i_b \,|^\gamma \tag{3.18}$$

when $0 < \gamma < 1$, occur when $i_b \neq 0$ only on the bonds of a spanning tree. The tree must be spanning due to constraints (3.16): you cannot have $i_b = 0$ for all b's incident on a site so that there must be at least one outlet from each site x. Some site must be declared to be a global outlet.

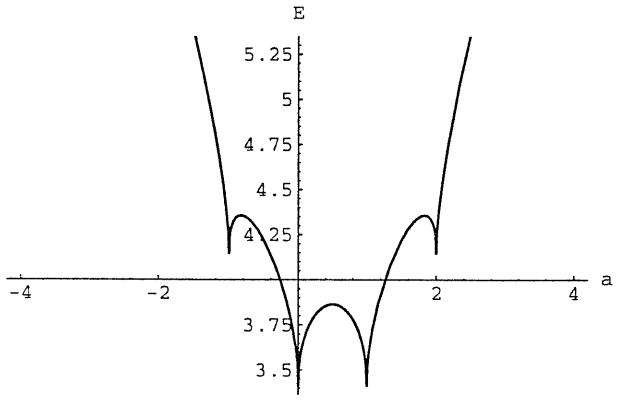

Figure 3.5: Plot of the function E versus a for $\gamma = 0.5$.

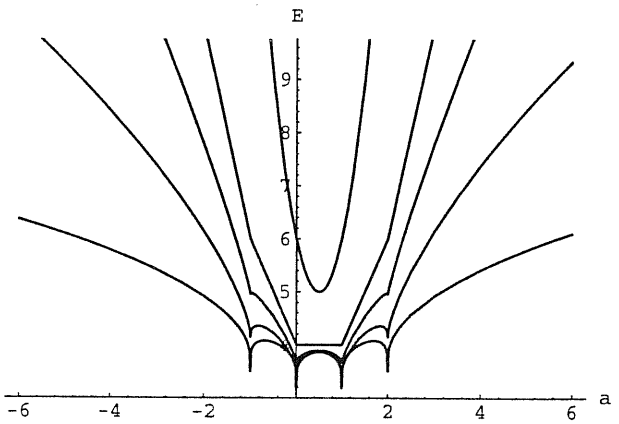

Figure 3.6: Plot of the function E versus a for $\gamma = 0.25, 0.5, 0.75, 1, 2$

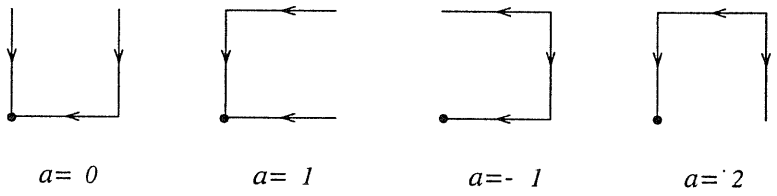

Figure 3.7: Loopless configurations for the graph of figure 3.8.

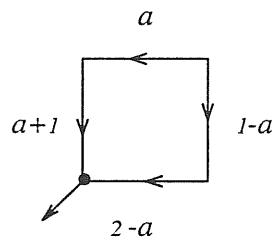

Figure 3.8: Example: graph with 4 bonds. The black dot is the outlet.

Thus loopless structures comes out as optimal structures of equation (3.18) with the constraint (3.16).

Let us start with an extremely simple example: 4 sites. After implementation of (3.16), in the notations of fig. 3.8, equation (3.18) becomes

$$E = \mid a \mid^{\gamma} + \mid a+1 \mid^{\gamma} + \mid 1-a \mid^{\gamma} + \mid 2-a \mid^{\gamma} . \tag{3.19}$$

In figure 3.5 one immediately sees that there are local minima in correspondence with one of the four currents being zero ($a = 2, 1, 0, -1$), corresponding to the four trees shown in fig. 3.7. The explanation is simple. Suppose that $a \sim 0$ (the other cases are equivalents). Then all the terms in (3.19) but $\mid a \mid^{\gamma}$ can be expanded in Taylor series around $a = 0$. Thus, locally

$$E = 2 + 2^{\gamma} + \mid a \mid^{\gamma} + \mathcal{O}(a) \tag{3.20}$$

which looks like a cusp, since $0 < \gamma < 1$; if $\gamma < 0$ there would be an asymptote instead of the cusp. Notice that $\frac{\partial E}{\partial a} \mid_{a=0^{\pm}} = \pm\infty$ and thus one cannot find the minima simply by imposing that $\frac{\partial E}{\partial a} = 0$. If $a \neq 0, \pm 1, 2$, being $\frac{\partial^2 E}{\partial a^2} < 0$ there are no other minima of E (only maxima).

In fig. 3.6 the function E versus a is plotted for various values of γ. Note that for $\gamma = 1$ all *directed* (with the currents going in the positive directions) configurations, loopless or

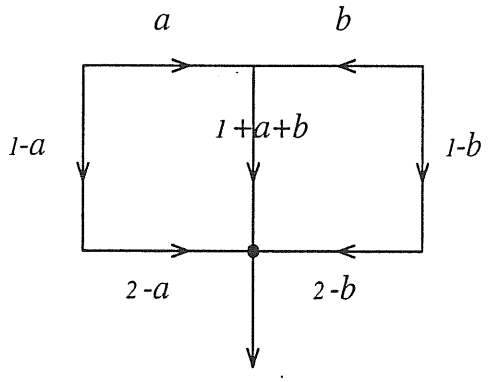

Figure 3.9: Example: graph with 7 bonds. The black dot is the outlet. A conventional orientation has been fixed on the bonds.

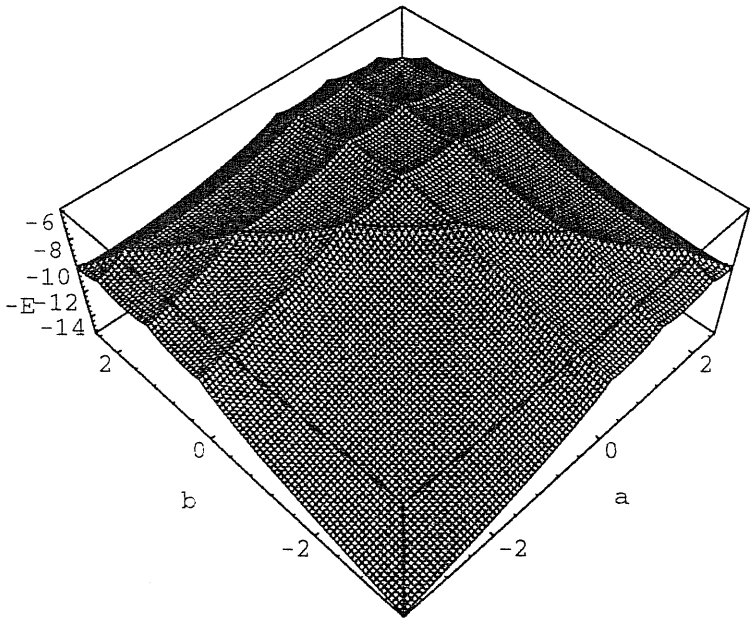

Figure 3.10: Plot of the function $-E$ versus (a, b) for $\gamma = 0.5$.

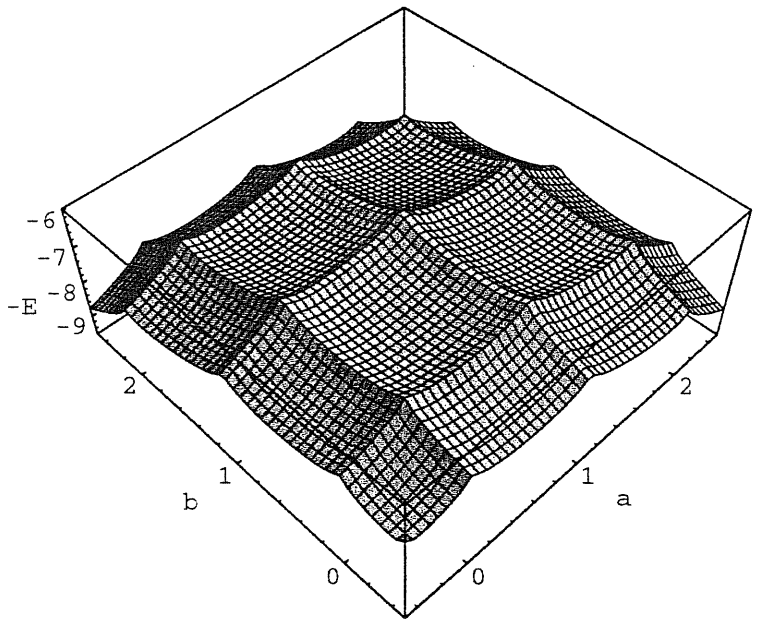

Figure 3.11: Detail of the plot of the function $-E$ versus (a, b) for $\gamma = 0.5$.

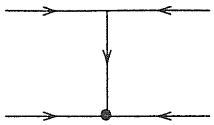

(a,b)= (1,1)

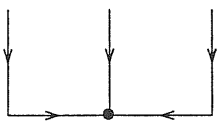

(a,b)= (0,0)

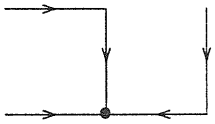

(a,b)= (1,0)

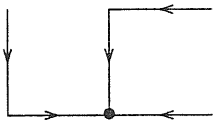

(a,b)= (0,1)

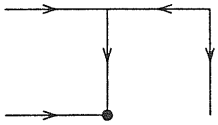

(a,b)= (1,2)

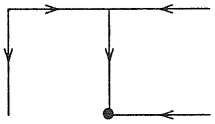

(a,b)= (2,1)

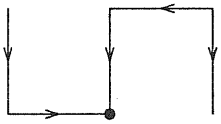

(a,b)= (0,2)

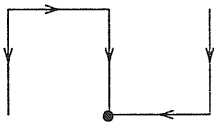

(a,b)= (2,0)

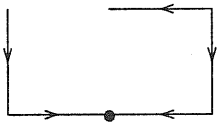

(a,b)= (0,-1)

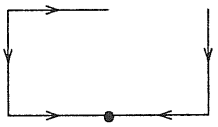

(a,b)= (-1,0)

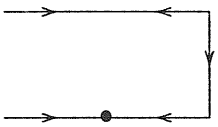

(a,b)= (1,-2)

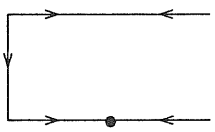

(a,b)= (-2,1)

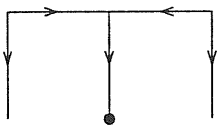

(a,b)= (2,2)

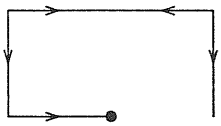

(a,b)= (-3,2)

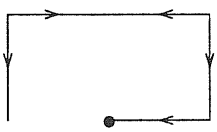

(a,b)= (2,-3)

Figure 3.12: The 15 loopless configurations for the graph of figure 3.9. The spanning trees with the same energy are on the same line and the lines are in the order of increasing energy. The arrows are drawn following the orientation fixed in fig. 3.9.

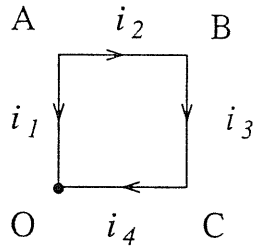

Figure 3.13: Signes of the current for the example with Lagrange multipliers.

not, have the same energy. The case $\gamma = 2$ corresponds to the resistor networks case in which there is just one minimum at $a = 1/2$.

Another example is that of the graph shown in fig. 3.9. The energy surface is shown in figures 3.10–3.11 (to make the cusps better stand out, we plotted $-E$ instead of E). The 15 cusps correspond to the 15 loopless configuration of this graph (see fig. 3.12). Note that since there is one unknown current for each bond and one continuity equation for each site the number of independent variables is given by the number of bonds minus number of sites (excluding the outlet).

3.4.2 Lagrange multipliers

Since we have seen that local minima occur in singular point configurations, where some currents are zero, we cannot introduce the standard technique of Lagrange multipliers to find the minima of E with the constraint (3.16). In order to be able to do that we must regularize E as follows

$$E = \sum_b (i_b^2 + \varepsilon^2)^{\gamma/2} \tag{3.21}$$

The previous definition is obtained in the limit $\varepsilon \to 0$. If we consider again the simplest case of the 4 bonds graph, we should solve the following equations (with i_1, i_2, i_3 and i_4 as in fig. 3.13).

$$0 = \frac{\partial}{\partial i_b}(E + \lambda_A(i_1 + i_2 - 1) + \lambda_B(i_3 - i_2 - 1) + \lambda_C(i_4 - i_3 - 1)) \quad , b = 1,2,3,4 \tag{3.22}$$

These imply (defining $\lambda_0 = 0$)

$$\begin{aligned}
\lambda_0 - \lambda_A &= \frac{i_1}{(i_1^2+\varepsilon^2)^{1-\gamma/2}}\gamma \ , && \text{(3.23a)}\\
\lambda_B - \lambda_A &= \frac{i_2}{(i_2^2+\varepsilon^2)^{1-\gamma/2}}\gamma \ , && \text{(3.23b)}\\
\lambda_C - \lambda_B &= \frac{i_3}{(i_3^2+\varepsilon^2)^{1-\gamma/2}}\gamma \ , && \text{(3.23c)}\\
\lambda_0 - \lambda_C &= \frac{i_4}{(i_4^2+\varepsilon^2)^{1-\gamma/2}}\gamma \ . && \text{(3.23d)}
\end{aligned} \tag{3.23}$$

If we define the r.h.s. of equations (3.23 $a-d$) as J_i then from equation (3.23) we have

$$-J_1 + J_2 + J_3 + J_4 = 0 \tag{3.24}$$

meaning that the *current* J_b is irrotational (i.e. $\vec{\nabla} \times \vec{J} = 0$ or equivalently $\oint d\vec{l} \cdot \vec{J} = 0$ around any loop). This, of course, has been allowed by the regularization that avoid that some $J_b \to 0$, corresponding to some $i_b \to 0$. If $\mid i_1 \mid \ll \varepsilon$, equations (3.23 $a-d$) have a solution

$$\begin{aligned} i_1 &= 1 + \mathcal{O}(\varepsilon^2) \\ i_2 &= \tfrac{\varepsilon^{2-\gamma}}{2^{1-\gamma}} \\ i_3 &= 1 + \mathcal{O}(\varepsilon^2) \\ i_4 &= 2 + \mathcal{O}(\varepsilon^2) \ , \end{aligned} \tag{3.25}$$

and

$$-\lambda_A = \gamma \ , \quad -\lambda_B = \gamma(1 + 2^{\gamma-1}) \ , \quad -\lambda_C = \gamma 2^{\gamma-1} \ , \tag{3.26}$$

and thus no divergence occurs on the r.h.s. of (3.23a). $-\lambda$ may then be identified as the height field. However the current directions do not correspond to the steepest descent.

It is indeed remarkable that if we take a subset of the set of all minima consisting in those spanning tree that are local minima of the functional (3.2), the current flow in the direction of the steepest descent. This follows directly from our proof of section 3.2 that reconstructing the elevation field from a spanning tree that is OCN local minima, and following the steepest descents, one gets back the same tree.

3.4.3 General Proof

Given an arbitrary graph, the number l of independent loops is given by

$$\#(\text{loops}) = \#(\text{bonds}) - \#(\text{sites}) + \#(\text{connected components}) \tag{3.27}$$

As was observed previously, our graphs must be spanning structures, thus #(connected components)= 1. For example, in the case of an $n \times m$ rectangular lattice, $l = nm - n - m + 1$. We want to show that any spanning tree is a local minimum of (3.18) and that there are not other minima.

The proof is easy if one fix a spanning tree and properly choose the independent variables to be the current flowing in the bonds absent in that tree.

Consider a general structure with l independent loops. The energy

$$E = \sum_b (i_b^2 + \varepsilon^2)^{\gamma/2} \tag{3.28}$$

has a local minimum in all the configurations T corresponding to currents $i_b \sim \varepsilon^{2-\gamma}$ in all $b \notin T$. If we overlap T to that structure, we can assign loop currents $x_1, x_2, ..., x_l$ to the bonds $b \notin T$. All the others currents are determined by the constraints (3.16) in terms of

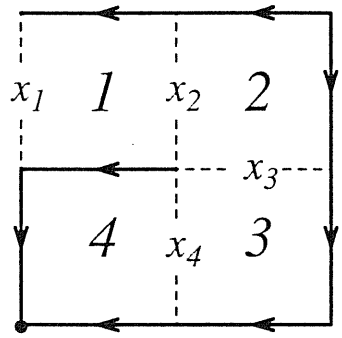

Figure 3.14: Spanning tree: the currents x_1, x_2, x_3 and x_4 in the four missing bonds are chosen as independent variables.

$\vec{x}$. Thus $E = E(\vec{x})$. We will prove that $\partial E/\partial x_i = 0$ at $x_i \sim \varepsilon^{2-\gamma}$ and that the Hessian is positive definite. Indeed

$$\frac{\partial E}{\partial x_i} = \gamma \sum_b \frac{i_b}{(i_b^2 + \varepsilon^2)^{1-\gamma/2}} \frac{\partial i_b}{\partial x_i}, \tag{3.29}$$

where i_b is linear in x_i and $\frac{\partial i_b}{\partial x_i} = \pm 1$. Notice that in the sum (3.29) not all the bonds b are necessarily present. For example in the case shown in figure 3.14 in $\partial E/\partial x_1$ it is absent at least the contribution from the bonds x_2, x_3 and x_4. This implies that only in one term of (3.29) $i_b \sim 0$ and it corresponds to $i_b = x_i$. All the others are finite when $\vec{x} \to 0$. Then, $\frac{\partial E}{\partial x_i} = 0$ implies

$$x_i = -\varepsilon^{2-\gamma} \sum_b{}' \mid i_b \mid^{\gamma-1} \operatorname{sgn}(i_b) \frac{\partial i_b}{\partial x_i} \propto \varepsilon^{2-\gamma} \tag{3.30}$$

and the sum $\sum'$ is over all the terms present in (3.29) but b: $i_b = x_i$.

$$H_{ij} = \frac{\partial^2 E}{\partial x_i \partial x_j} = \gamma(\gamma - 1) \sum_b{}'' \mid i_b \mid^{\gamma-2} \frac{\partial i_b}{\partial x_j} \quad i \neq j, \tag{3.31}$$

where in the $\sum''$ the contributions from b: $i_b = x_k$ are absent. Thus $\frac{\partial^2 E}{\partial x_i \partial x_j}$ are finite in the $\varepsilon \to 0$ limit. When $i = j$

$$H_{ij} = \frac{\partial^2 E}{\partial x_i \partial x_j} = \gamma \varepsilon^{\gamma-2} + \mathcal{O}(\varepsilon^{-\gamma}), \tag{3.32}$$

and thus H has the form

$$H = \gamma \varepsilon^{\gamma-2} (\mathit{1\!I} + \varepsilon^{2-\gamma} T), \tag{3.33}$$

where $T_{ii} = 0, T_{ij} = H_{ij}$ $i \neq j$. This implies that the eigenvalues of H, for sufficiently low ε are all positive, meaning that (3.30) is indeed a minimum.

Moreover one can see that closing one or more loops with finite currents (taking one or more x_i finite) causes the appearance of one negative eigenvalue in the Hessian matrix

for each added bond. If x_i is the current in this added bond, then the first derivative is $\frac{\partial E}{\partial x_i} = \gamma \mid x_i \mid^{\gamma-1} \mathrm{sgn}(x_b) + \gamma \sum_b' \mid i_b \mid^{\gamma-1} \frac{\partial i_b}{\partial x_i} \mathrm{sgn}(x_b)$, and the second derivative is $\frac{\partial^2 E}{\partial x_i^2} = \gamma(\gamma-1) \mid x_i \mid^{\gamma-2} + \sum_b' \gamma(\gamma-1) \mid i_b \mid^{\gamma-2} < 0$. Being $H_{kk} < 0$ implies that $\sum_{ij} H_{ij} z_i z_j < 0$ if $z_k \neq 0$ and $z_i = 0, i \neq k$. This shows that in this case the quadratic form H_{ij} is not positive definite and no local minima can be found when there are loops with finite currents in the $\varepsilon \to 0$ limit. This completes the proof.

When Lagrange multipliers are introduced

$$0 = \frac{\partial}{\partial i_b}\left[E + \sum_x [(\partial i)_x - 1]\lambda_x \gamma\right] = \gamma\left[\frac{i_b}{(i_b^2+\varepsilon^2)^1 - \gamma/2} - (d\lambda)_b\right], \tag{3.34}$$

where $(d\lambda)_b = \lambda_x - \lambda_y$ if b links x and y. From equation (3.34)

$$(d\lambda)_b = \frac{i_b}{(i_b^2+\varepsilon^2)^1 - \gamma/2}. \tag{3.35}$$

Corresponding to a given tree T for the i_b with $b \in T$, since $i_b \neq 0$, we have

$$(d\lambda)_b = \mid i_b \mid^{\gamma-1} \mathrm{sgn}(i_b) + \mathcal{O}(\varepsilon^{2-\gamma}), \tag{3.36}$$

whereas, for $b \notin T$

$$(d\lambda)_b = \frac{i_b}{(i_b^2+\varepsilon^2)^1 - \gamma/2} = -\sum_b' \mathrm{sgn}(i_b) \frac{\partial i_b}{\partial x_i} \mid i_b \mid^{\gamma-1}, \tag{3.37}$$

where the sum has the same meaning as in (3.30).
Notice that the neglected terms in (3.36) come from the x_i dependence of i_b.

Let us verify that (3.36) and (3.37) are consistent. With reference to the figure 3.15 we have that all bond on the side (1) have a current $i_b \to i_b + x$ when $x = 0 \to x \neq 0$, whereas on the side (2) $i_b \to i_b - x$. On the side (3) the currents do not depend on x. Thus

$$(d\lambda)_{b^*} = -\sum_{b \in \text{side 1}} \mid i_b \mid^{\gamma-1} \mathrm{sgn}(i_b) + \sum_{b \in \text{side 2}} \mid i_b \mid^{\gamma-1} \mathrm{sgn}(i_b), \tag{3.38}$$

$$\begin{gathered} 0 = \textstyle\sum_{b \in \text{side 1} \cup (-\text{side 2}) \cup b^*} (d\lambda)_b = \\ \textstyle\sum_{b \in \text{side 1}} \mid i_b \mid^{\gamma-1} \mathrm{sgn}(i_b) - \sum_{b \in \text{side 2}} \mid i_b \mid^{\gamma-1} \mathrm{sgn}(i_b) + (d\lambda)_{b^*}, \end{gathered} \tag{3.39}$$

is indeed satisfied due to equation (3.38).

This also shows that the terms contributing to equation (3.37) are the ones along the unique path of T joining the extrema of the bond creating the loop.

3.4.4 Case $\gamma = 1$

In the case $\gamma = 1$ the previous proofs does not hold. However one can proof that in that case, all *directed* configurations, i.e. in which the currents flow in the positive directions

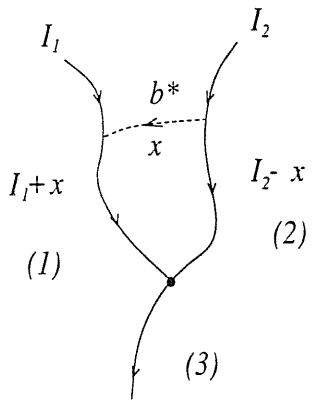

Figure 3.15: Notations for the last part of the proof.

correspond to the same energy, and that any other configuration has a bigger energy. You can see that in the simple example of one loop in fig. 3.6.
The proof goes like follows: Let us call $V(x)$ the distance of site x from the outlet. Any site y nearest neighbourg of x and flowing into x has a distance $V(y) = V(x) + 1$ from the outlet. Then

$$\sum_x V(x) = \sum_x V(x)(\partial i)_x = \sum_b i_b(\partial V)_b = \sum_b i_b\,, \tag{3.40}$$

where the $\sum_x$ is a sum over the sites and $\sum_b$ is a sum over the bonds. Note that $\sum_x V_x$ depends only on graph topology and is independent on currents configuration.
If the configuration is directed, then $\sum_b i_b = \sum_b \mid i_b \mid \doteq E_d$, since oll currents are positive. In any other currents configuration

$$E = \sum_b \mid i_b \mid \geq \left|\sum_b i_b\right| = \sum_x V_x\,, \tag{3.41}$$

and then $E \geq E_d$. This completes the proof.

3.5 Feasible Optimality

In two complex optimization problems related to the evolution of fluvial networks [37, 38, 39] and the geometry of domain walls in random ferromagnets [40], key statistical features of the global optima are exactly known [17, 40, 41, 42]. In the first case extensive experimental observations are also available [43, 44, 45, 21, 25, 24]. Imperfect optimal search procedures [46, 47] yield local optima statistically indistinguishable from those observed in Nature and quite different from the global solutions. Instead, more refined annealing procedures [14, 30] achieve optimal states closer to the actual ground state but with significant departures from natural structures.

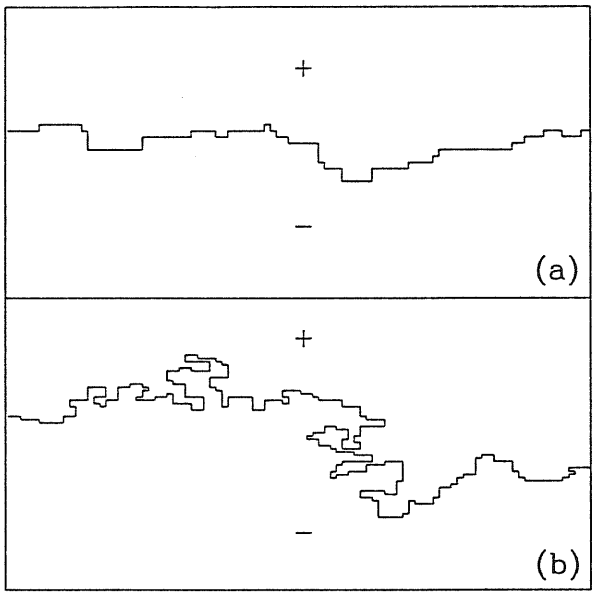

Figure 3.16: (a) The shape of the ground state interface of a two-dimensional random ferromagnet bounded by + and − boundary conditions respectively at the top and bottom faces of a two-dimensional lattice of size 96 × 96. The domain wall between regions of different magnetization is highlighted. It is a self-affine curve with wandering exponent H equal to 2/3 (i.e. if L is the linear size of the system, the vertical fluctuations Y of the self-affine curve scale like $Y \propto L^H$); (b) feasible domain wall, obtained by a $T = 0$ search for minimum total energy (i.e. flipping only the randomly chosen spins actually lowering total energy). Regardless of initial conditions, the domain wall is a robust self-similar curve characterized by fractal dimension $D = 1.6$ (if the actual curve length is ℓ the scaling relationship is $\ell \propto L^D$) .

The optimization problem defined by the OCN model, consists on choosing the network whose energy dissipation function is lowest, and entails an involved selection procedure among the exponentially large number of spanning networks in a given domain. As we have already pointed out, the statistical attributes of the global minimum are known exactly [17], and does not agree at all with the great amount of data available from Nature . Spanning, loopless network configurations realizing local minima of the energy dissipation (OCNs) show instead many interesting properties of fractality and a striking resemblance to river landforms in Nature [37, 38, 39, 17, 48, 49, 50].

The same features can be observed in a completely different context, i.e. in the problem of domain walls in random ferromagnets. Consider a ferromagnet in a box, with + and − boundary conditions at the top and at the bottom faces. The energy at $T = 0$ depends only on the shape of the interface between the + and − regions, and its minimum is

realized when the interface is flat (the position of course does not matter). In a random exchange ferromagnet at sufficiently low temperatures, the interface between regions of different magnetization is no more flat, but it is self-affine [40] (Fig. 3.16 (a)). In two-dimensional random-ferromagnets, it is known [40, 41, 42] that the roughness exponent of the self-affine interface (the domain wall) optimum is 2/3. With local zero-temperature spin-flip dynamics (i.e. spins are updated only if the global energy decreases), we have found that the global minimum is never reached and the domain walls are self-similar rather than self-affine (Fig. 3 (b)) with a fractal dimension around 1.6. This result is robust and independent if one adopts a single or two spin flip dynamics and whether one uses a discrete spin model or a continuum Langevin equation. Moreover, it ought to be amenable to experimental confirmation in direct probes of the domain wall geometry in deep quench spinodal decomposition measurements on random exchange metals.

Thus it seems in this two examples that river networks and domain walls in random ferromagnets are not free to explore extended regions of their fitness landscapes, suggesting that Nature might not search for global minima when striving for optimality.
This might indeed be true for many optimal configurations of a physical system that minimize a cost function arising in a variety of contexts.

4 Random Aggregation and Diffusive Coalescence

In an aggregation phenomenon, diffusive particles join whenever they meet. This is one of the most typical irreversible processes and has always attracted much attention since the seminal works of Smoluchowski [51].
Since aggregation processes are one of the simplest non-thermal equilibrium phenomena, their understanding is of fundamental importance for the construction of a theory of statistical physics out of equilibrium.
Moreover they are relevant in many fields of science and technology, for example in colloid science and polymerization.

In this chapter we describe a random aggregation model with injection proposed by Takayasu [52], who gave the solution in $d = 1$ and in mean field.
We show how its solution in arbitrary dimensionality can be obtained by an exact mapping on a reaction process.

In the first section we briefly review the Takayasu model, the Scheidegger rivers model [4] (equivalent to the Takayasu in $d = 1$) and the coalescence process.
In the second section we show that this random aggregation model is related to the coalescence process through an exact mapping. Scaling relations may be derived, and allow to get the solution in arbitrary dimensionality. The upper critical dimension is found to be 2. Moreover, randomness in injection with a finite first moment is shown to be irrelevant.

4.1 Random Aggregation and related models

4.1.1 Takayasu Model of Random Aggregation

Takayasu and collaborators[52, 53, 53] have shown that models of random aggregation with *constant* injection of particles exhibit a power-law mass distribution asymptotically in time. The random aggregation model has been solved exactly in 1+1 dimension [52, 54] and within

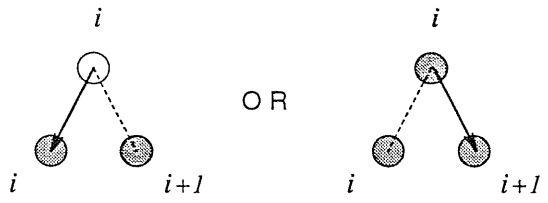

Figure 4.1: In $d = 1$ the particle at the i^{th} site stay at i or jumps to the $(i+1)^{th}$ site with probability 1/2.

the mean field approximation valid in dimensionalities greater than or equal to the upper critical dimension.
This model is additionally related to a large class of dynamical models including the voter model [55], a directed model of self organized criticality [56] and critical branching models [57].
In the $D = d+1$ random aggregation model [52], particles with unit mass are initially placed on each site of a d dimensional lattice. At each time step, the particles independently jump to a randomly chosen site according to a given probability.
Whenever particles end up on the same site, they aggregate to form just one particle with conserved mass. Each time step, particles with unit mass are injected on to every site.
This procedure of diffusion, aggregation and injection is then repeated. The diffusional process is assumed to be independent of the mass of the diffusing particle.

The dynamic is described by the following set of equations relating the mass of the particle at each site at time step $t+1$ to the masses at time step t:

$$M_i(t+1) = \sum_j W_{i,j}(t) M_j(t) + r_i, \tag{4.1}$$

where $W_{i,j}(t)$ are random variables given by

$$W_{i,j} = \begin{cases} 1 & \text{with probability } 1/D \quad \text{for } i-j = \hat{0}, \hat{1}, .., \hat{d} \\ 0 & \text{otherwise} \end{cases} \tag{4.2}$$

where $\hat{0}$, ..., $\hat{d}$ are the unit vectors along coordinate axis. In the case of uniform injection $r_i(t) = 1$, $\forall i$, t. This corresponds to a particle staying still or moving along the positive direction of a coordinate axis[1] with equal probability (fig. 4.1). An example of this dynamic is shown in figure 4.2.

An infinite range mean field version of the model is obtained on replacing equation (4.2) with

$$W_{i,j} = \begin{cases} 1 & \text{with probability } 1/N \\ 0 & \text{with probability } 1 - 1/N \end{cases} \tag{4.3}$$

[1] As far as $W_{i,j}$ is short range, the critical exponents should remain the same as for the choice (4.2).

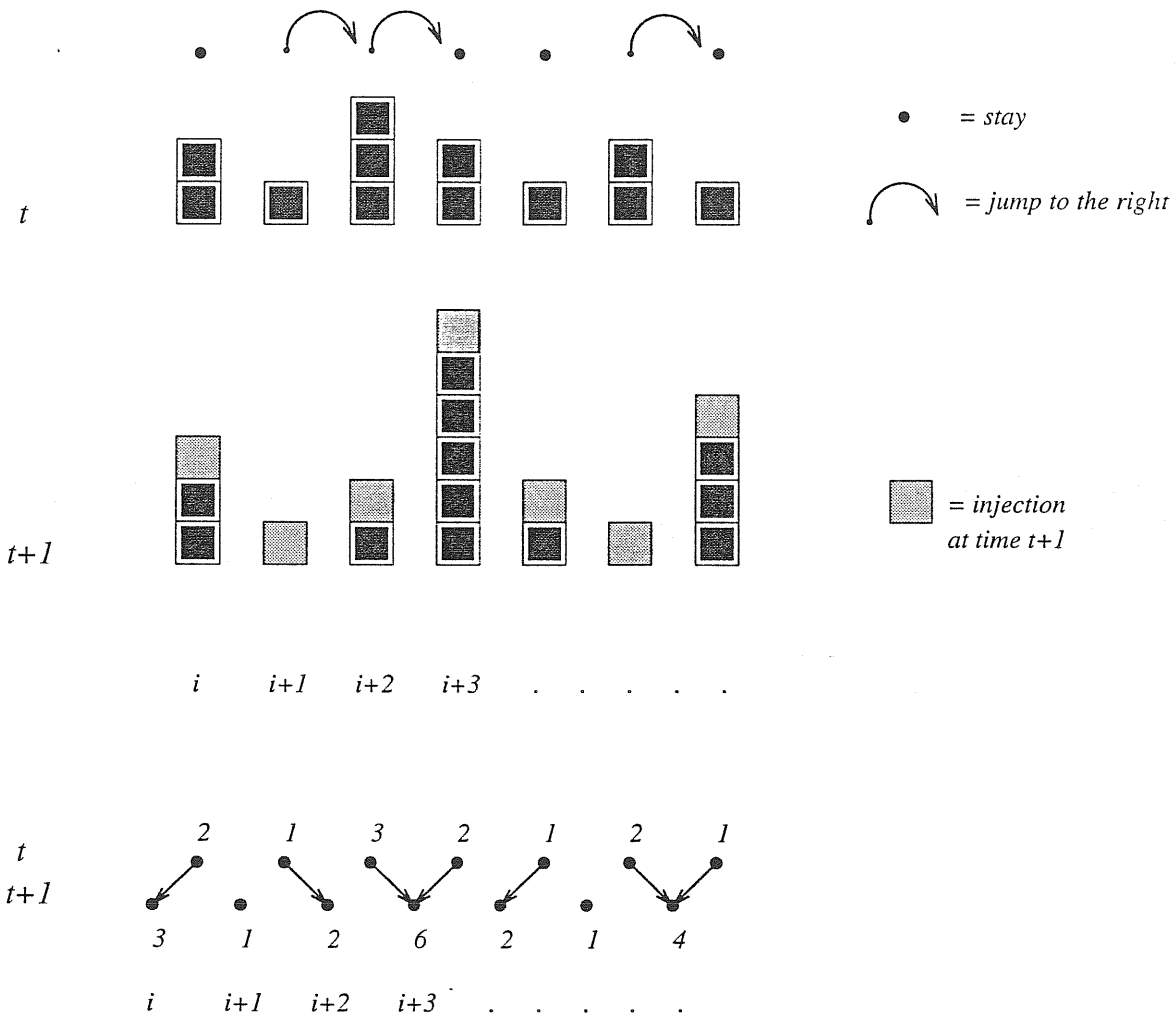

Figure 4.2: Example of dynamics for the aggregation model.

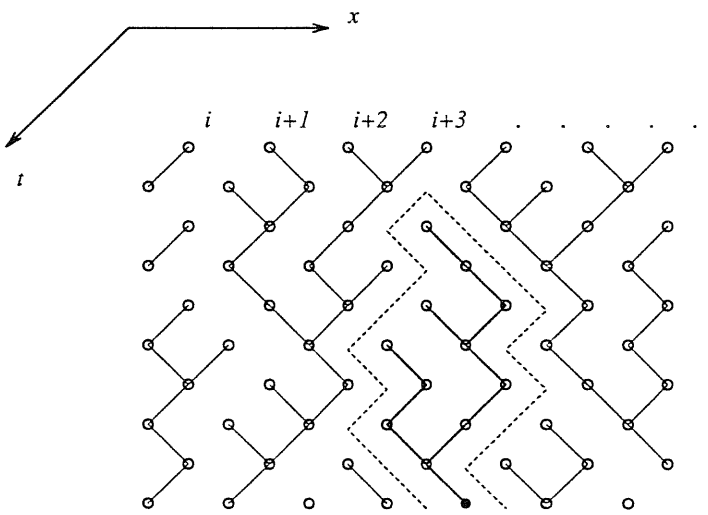

Figure 4.3: Example of patterns formed by the aggregation process with injection in $d = 1$. The particle mass at the black site is equal to the area inside the dotted region.

for every i and j, where N is the total number of sites. It is known[52] that at long times, the distribution of masses is characterized by a power law.

The exponents in $D = 1+1$ can be deduced in a simple manner by an intuitive geometrical argument: roughly speaking the particle mass M at a given point i is proportional to the area bounded by two random walk trajectories (see fig. 4.3). Since the width of that region is expected to be proportional to the square root of the height h, one finds that the mass at the point i is given by[2]

$$M(T) \propto T^{\Phi}\,, \text{ with } \Phi = 3/2\,. \tag{4.4}$$

Since h can be regarded as the first collision time of two random walks, its distribution $p(h)$ is approximatively given in $d = 1$ by the well known expression:

$$p(h) \simeq (2\pi)^{-1/2} e^{-1/2\,h} h^{-3/2}\,. \tag{4.5}$$

Combining equations (4.4) and (4.6) one gets for the probability to have a mass M bigger than s the expression

$$P(M \geq s) \propto s^{-1/3}\,. \tag{4.6}$$

The rigorous solution for $d = 1$ given by Takayasu [52] goes like follows: consider the distribution of particle mass $P(M \geq s)$. The asymptotic behaviour for $s \gg 1$ corresponds to that of the characteristic function

$$Z(\rho, t) = \langle e^{-\rho s} \rangle = \sum e^{-\rho s} \rho(s, t) \tag{4.7}$$

[2] On naively generalizing to dimension $D = d + 1$, one obtains $\Phi = 1 + d/2 = \psi$ and $\tau = 2(1+d)/(2+d)$. The mean field [52] values, $\Phi = 2 = \psi$ and $\tau = 3/2$, are obtained in $d = 2$ suggesting that it is the critical dimension.

for $\mid \rho \mid \ll 1$. Let us introduce the r bodies characteristic function

$$Z_r(\rho, t; i_1, ...i_r) = \langle e^{-\rho(s_{i_1}+\cdots+s_{i_r})} \rangle \,, \tag{4.8}$$

where the average is on the stochastic variables $\{W_{i,j}(m), m = 0, 1, ..(n-1)\}$. In the short range case of equation (4.2) it is enough to consider $Z_r$for adjacent sites $i, i+1, ...i+r$. Equation (4.1) implies for the Z_rs:

$$Z_r(\rho, t+1) = \frac{e^{-\rho r}}{4}[Z_{r+1}(\rho, t) + 2Z_r(\rho, t) + Z_{r-1}(\rho, t)] \,. \tag{4.9}$$

Assuming the convergence $Z_{r+1}(\rho, t) \rightarrow Z_r(\rho)$ in the $t \rightarrow \infty$ limit:

$$Z_{r+1}(\rho) + (2 - 4e^{\rho r})Z_r(\rho) + Z_{r-1}(\rho) = 0, \;\; (Z_0 \doteq \langle 1 \rangle = 1) \,. \tag{4.10}$$

$Z_1(\rho)$ can be expressed in form of a continued fraction

$$Z_1(\rho) = \cfrac{1}{4e^{\rho} - 2 - \cfrac{1}{4e^{2\rho}-2-\cfrac{1}{4e^{3\rho}-2-\cdots}}} \tag{4.11}$$

that, for $\mid \rho \mid \ll 1$ becomes:

$$Z_1(\rho) = \cfrac{1}{2 + 4\rho - \cfrac{1}{2+8\rho-\cfrac{1}{2+12\rho-\cdots}}} \simeq 1 + c\rho^{\alpha} \,. \tag{4.12}$$

α can be computed numerically and results to be $\alpha \simeq 0.333..$ in accordance with the previous argument based on random walks that gives $\alpha = 1/3$.

For the mean field case, Takayasu solution is as follows. The time evolution for the mass distribution function $p(M, t)$ (probability to have a particle with mass M at time t) is given considering all possible realizations of the aggregation:

$$p(s+1, t+1) = \sum_{r=1}^{N} a_r \sum_{s_1+\cdots+s_r=s} \prod_{i=1}^{r} p(s_i, t) \,, \text{ with } p(1, t) = a_0 \,, \; (t \geq 0) \,. \tag{4.13}$$

where a_r denotes the probability that r particles come together at a site, and it is given by

$$a_r = \binom{N}{r} \left(\frac{1}{N}\right)^r \left(1 - \frac{1}{N}\right)^{N-r} \,, \; r = 0, 1, ..N \,. \tag{4.14}$$

The a_r satisfies the constraints of normalized probability conservation $\sum_{i=0}^{N} a_i = 1$, and the particle number conservation $\sum_{i=1}^{N} i\, a_i = 1$. Laplace transform of equation (4.13) gives the characteristic function

$$Z(\rho, t+1) = e^{-\rho} \sum_{r=0}^{N} a_r Z(\rho, t)^r \,. \tag{4.15}$$

If we assume the convergence to $Z(\rho)$ in the $t \rightarrow \infty$, equation (4.15) reduces to

$$Z(\rho) = e^{-\rho} \sum_{r=0}^{N} a_r Z(\rho)^r \,, \tag{4.16}$$

that may be expanded in terms of $y(\rho) = Z(\rho) - 1$ for $\rho \simeq 0$ and gives

$$Z(\rho) = 1 + y(\rho) = \left(1 - \rho + \frac{\rho^2}{2} - \cdots\right) \sum_{r=0}^{N} a_r [1 + y(\rho)]^r = \tag{4.17}$$

$$\sum_{r=0}^{N} a_r + \sum_{r=1}^{N} r\, a_r\, y(\rho) + \sum_{r=2}^{N} \frac{r(r-1)}{2}\, a_r\, y(\rho)^2 + \cdots . \tag{4.18}$$

Due to the constraints on the a_r, the coefficients of the terms of order zero and one in y in equation (4.18) vanish[3], thus

$$y(\rho) \propto \rho^{1/2}, \tag{4.19}$$

implying $P(M \geq s) \propto s^{1/2}$.

4.1.2 Scheidegger model

The Takayasu model in $d = 1$ is known to be equivalent to one of the earliest models of river networks [4]. It is worth discussing it since river networks are the main subject of this work.

The basic Scheidegger river model, was originally proposed by an hydrodynamic researcher, A. E. Sheidegger in 1967 to study river networks. In 1986 it has been "reinvented" (is the word used by the authors) as a model of random aggregating particles by physicists [58], and in 1989 has been solved by Takayasu [52].

Let us picture a slope with many bulges, under a rain (see figure 4.4). Raindrops fall uniformly and they flow along the slope. When a stream of water encounters a bulge, it slides down to the left or to the right randomly. When two streams happen to gather at the same point, they coalesce and continue to glide down. Once a path has been created, all later raindrops that come upon it follow the same rout. If the surface is large enough, after some time we will see a hierarchy of little streams and rivulets.
The essential points of this picture can be formulated in a simple discrete model.
On a hyper-cubic lattice, the river networks are defined to be a set of spanning trees along which water is transported from each of the sites to the outlet sites defined to be that on the hyper-plane given by, say, $z = 0$. Locally, water at a site with a given z coordinate z_0 is assumed to flow to a site with $z = z_0 - 1$; the flow is directed. The time axis in the random aggregation model corresponds to the spatial z-axis in the Scheidegger problem and thus the aggregation model in dimension d is equivalent to a river basin in $D = d+1$ dimensions. Equation (4.2) describes the situation in which water from any given site flows locally to one of the nearest neighbourg sites in the hyper-plane below it with equal probability whereas

[3] Note that if the conservation of particles number is violated, the coefficient of the term of order 1 in y in equation (4.18) does not vanishes, implying $y \propto \rho$. As a consequence there will be an exponential decay in the mass distribution, revealing the essential role of injection to get power law distribution of masses.

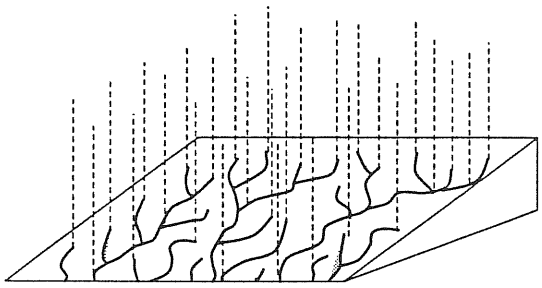

Figure 4.4: Rivers pattern on the slope.

the mean field version (equation (4.3)) corresponds to water flowing to any site in the hyperplane below with equal probability. The particle mass in the random aggregation model corresponds to the accumulated area of the aggregating water, while the injection captures the rainfall on the individual sites.

In figure 4.3 the particles at the last row have masses equal to the area of the drainage basin of the corresponding branching structure, since we inject an unit mass particle per one time step at every site.

A sort of reversed version of the Scheidegger model is the voter model, a simple model for the formation of public opinion. The sites of a one dimensional lattice are occupied by persons who are either in favor or in opposed to some issue. The voters could change their opinion by the influence of their neighbours. This is equivalent to a particle system in which a particle at a certain time changes its state to one of the neighbouring particle's state stochastically. After a long time, the particles having the same state start forming clusters in one-dimensional lattice, similar to patterns in a reversed Scheidegger network.

4.1.3 Coalescence Process

In the next section we will show that there exists an exact mapping between the Takayasu random aggregation model and the diffusive coalescence process $A + A \rightarrow A$.

This is a process in which each A particle independently follows a random walk. When two particles end up on the same site, they aggregate to form just one particle. Note that this model is identical to the random aggregation model except for one crucial difference. Unlike the aggregation model, here there is no injection of particles. Indeed, in the diffusive coalescence model, at long times, one ends up with just one particle. The concentration of A particles at time t is

$$c(t) = \frac{N(t)}{V}, \tag{4.20}$$

where $N(t)$ is the number of particles and V is the total number of sites. The asymptotic

behaviour of $c(t)$ as been solved exactly [59] leading to

$$c(t) \sim \begin{cases} t^{-d/2} & d < 2 \\ t^{-1} \log t & d = 2 \\ t^{-1} & d > 2 \,. \end{cases} \tag{4.21}$$

A simple way to understand this is as follows. In an interval Δt, $N(t)$ is decreased by the number of "collisions" that occur during this time. Let $s(t)$ denote the number of distinct sites visited by a given particle until time t. The number of collisions of the particle is proportional to the number of particles in a volume $\Delta s(t)$. The total number of collisions is therefore proportional to $N(t)c(t)\Delta s(t)$. Thus

$$N(t) - N(t + \Delta t) \sim N(t)c(t)\Delta s(t) \,. \tag{4.22}$$

On dividing by V and in the limit $\Delta t \to 0$ one gets

$$-\dot{c}(t) \sim c^2(t)\dot{s}(t) \,, \tag{4.23}$$

and thus

$$c(t) \sim \frac{1}{s(t)} \,. \tag{4.24}$$

The number of distinct sites visited by a random walker in d dimensions has been worked out in [60, 61, 62] and yields the aforementioned result.

4.2 Mapping of the Random Aggregation Model on the $A + A \to A$ Reaction

In this section, we establish a link between the random aggregation model and the problem of diffusive coalescence. This enables us to solve the random aggregation model in arbitrary dimensionality. An important byproduct of our solution is that we are able to show that the upper critical dimensionality is $D = 2 + 1$ and explicitly determine the logarithmic corrections to the power law behavior at the upper critical dimension. We are also able to prove that random injection with a finite first moment does not change the universality class in any D.

It is known[52] that at long times, the distribution of masses is characterized by a power law. Motivated by our studies [63, 64, 17, 14] of river networks, we define a quantity analogous to upstream lengths for each site i as the *age of the oldest particle* constituting the composite particle at that site. We denote this by X_i. We proceed to make a scaling ansatz [10] as in section 5, chapter 2, for the probability density distributions of the masses M and the ages X defined above:

$$p(M, T) = M^{-\tau} f(M/T^{\Phi}) \,, \tag{4.25}$$

$$\pi(X,T) = X^{-\psi} f(X/T)\,, \tag{4.26}$$

where T is the total number of time steps. Recognizing that the mean mass (averaged over each of the sites and for all the T time steps) ought to be proportional to T (the proof is given later in equation (4.32) for a more general case) and requiring that $p(M,T)dM = \pi(X,T)dX$ [4], with $X \sim T \sim M^{1/\Phi}$ one obtains

$$\Phi(2-\tau) = 1 \quad \text{and} \quad \psi = \Phi. \tag{4.27}$$

In order to calculate the ψ exponent for the age distribution, we have to evaluate the fraction of sites whose composite particle is constituted from at least one particle of age greater than T.

This problem is directly related to one of evaluating the density of particles surviving a diffusive annihilation $A + A \rightarrow A$ process after a time $t = T$. Indeed, the probability $P(X \geq X_0) = c(X_0)$ so that the probability density $\pi(X_0) = dP(X \geq X_0)/dX_0$ is given by

$$\pi(X_0) \sim \begin{cases} X_0^{-(d/2+1)} & d < 2 \\ X_0^{-2} \log X_0 & d = 2 \\ X_0^{-2} & d > 2\,. \end{cases} \tag{4.28}$$

Thus, from the relation between the exponents, we deduce that $\psi = \Phi = d/2 + 1$ and $\tau = \frac{2(d+1)}{(d+2)}$ for $d < 2$ and $\psi = \Phi = 2$ and $\tau = 3/2$ for $d \geq 2$. Alternatively, the Φ exponent relating the mass M of a particle, with the time T, can be deduced as follows.

Given a space-time point O, let us consider the intersection of its basin (sites aggregating into O) with a $d-$dimensional spatial hyper-plane, a time t prior to O (see fig. 4.5). Be $N_\perp$ the typical number of points in this set. The masses on these sites aggregate, effectively following an $A + A \rightarrow A$ process, until the number of A particles becomes of order 1 after a time t. Thus

$$N_\perp(t)c(t) \sim 1. \tag{4.29}$$

The number of particles aggregated within a time interval T is then given by

$$M(T) \sim \int_0^T dt N_\perp \sim \int_0^T dt \frac{1}{c(t)} \sim \begin{cases} T^{1+d/2} & d < 2 \\ \frac{T^2}{\log T} & d = 2 \\ T^2 & d > 2\,, \end{cases} \tag{4.30}$$

Logarithmic corrections to the power law behaviour of the distribution of masses in $d = 2$ can be evaluated using the age distribution and noting that $M \sim \frac{T^2}{\log T}$:

$$p(M) \sim \frac{\pi(T)}{dM/dT}\,|_{M \sim \frac{T^2}{\log T}} \sim \frac{\log^2 T}{T^3} \sim M^{-3/2}(\log M)^{1/2}\,. \tag{4.31}$$

[4] This follows in a trivial way on changing variables from M to X, provided M is a function of X. The same result also holds in a more general case where both M and X are random variables such that the conditional probability to find a value X, given a particular value of M, has a scaling form $\frac{1}{X}\, g(M^{\frac{1}{\Phi}} X^{-1})$.

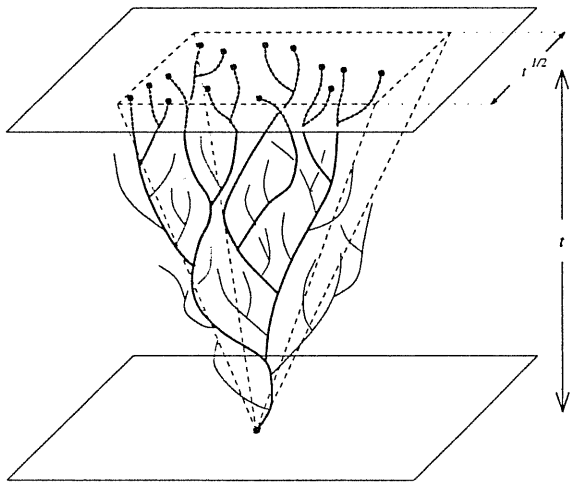

Figure 4.5: Sketch of the basin of attraction for the aggregation of particles constituting the composite particle at the site at the bottom. The time axis points downwards, the spatial hyper-plane is perpendicular to the time axis and contains $N_\perp(t)$ masses that aggregate to form a single mass at 0.

The relation between the aggregation model and the diffusive annihilation model still holds in the case of random injection, i. e. in the case in which in (1), $r_i(t)$ are independently distributed random variables ≥ 0. Moreover, the equations (4.27) can be deduced in this more general case.
Indeed, the mean mass (averaged over each of the sites and for all the T time steps) averaged over the randomness is given by

$$\begin{aligned} \langle M(T)\rangle = \quad & \lim_{L\to\infty}\langle \tfrac{1}{L^d T}\textstyle\sum_{i,t} M_i(t)\rangle = \lim_{L\to\infty} \tfrac{1}{L^d T}\textstyle\sum_{i,t}\sum'_{j,s<t}\langle r_j(s)\rangle \quad = \\ & \lim_{L\to\infty} \tfrac{1}{L^d T}\textstyle\sum'_{j,s}\langle r_j(s)\rangle(T-s) = \tfrac{1}{T}\langle r\rangle\textstyle\sum_s (T-s) = \tfrac{T-1}{2}\langle r\rangle \quad . \end{aligned} \tag{4.32}$$

In the third step $\sum'_j$ is restricted to sites j at time s whose mass is "collected" at site i at time t. Thus if $\langle r\rangle$ is finite, eq. (4.32) implies that the arguments used for the uniform injection case are still valid, the scaling laws in equation (4.27) hold and the exponents remain the same as before. Random injection with finite (non zero) $\langle r\rangle$ was already analyzed for the particular case $D = 1+1$ by Takayasu [65], and it was shown to be irrelevant by the explicit solution.

We conclude by noting that our results are generalizable to fractal geometries [66] with the spectral dimension playing the role of d.

5 Acknowledgments

First Edition

Here we are to the longest chapter:
there are a lot of people I wish to thank!

First of all, Erio Tosatti and all the CM sector for accepting me when I was a "stateless" (aspirant) physicist. They really gave me a great opportunity.
A special thank to Amos, for a lot of reasons:
for his extraordinary ability to place himself at your same level..whatever it is, and to be able to discover a clever idea in what you tell him... even if it is very very well hidden;
for being able to understand what you do not even realize to be saying (sometimes this make you feel so undeservingly smart!);
finally for all that I have learned from him (a lot of things!) in this year and a half, and for his contagious enthusiasm. In short, I could not wish more!
Thanks a lot to Jayanth Banavar and to Andrea Rinaldo for the very fruitful "long-distance collaboration". I hope it will go on!
Thanks to all other people with whom I have been collaborating during these years, our big brother Achille, Marek Cieplak and Michael Swift.
Thanks to all the SISSA staff, especially to Alex, Andrea (I know that you are reading me!!), Fabia and Riccardo, for being always so nice and efficient.
A special thank to Sabrina, of course.
Thank you to all the "statistical conscription 1996", Guido, Lucian, Michele, Paolo, Sandro (and I)! Any af you would deserve a special section but .. you all know .. I'm always late.
Thanks a lot to Franjio for having really saved my life with ispell.
Thanks to Franz (Robin) Di Tolla for having been my first interface with technology.
Thanks to all the "analysts", Piero (the pilgrim), Paolo (cal), and to Luca (billy) for the nice time spent together. In particular, thanks to Luca for the billions of notions that he gave me in he's spare time, and in particular for conceiving the $\alpha - \epsilon$ *method* that I will never forget.

Thanks a lot to Stefano (panz) for his efforts to understand my strange language and to Loredana.
Thanks to Gabriele for being so.
Thanks a lot to Giuseppe (the Champ), for revealing some of the secrets to become a Champ (...?), to Michela and, above all, to Chiara.
Thanks a lot to Juppy because in all these years nothing changed.
Thanks to Fabiana and Luigi for being close to me.
Thanks in random order to Laura, Carlo, Leonardo, Cecilia, Angelo, Vito, Claudio, Alessandro, Salvatore, Cristina, Francesco, ...
Finally, thanks Sandro, for having been always with me..
Thanks above all to all whom I forget, for what they did for me, and ...sorry!

Second Edition

Two acknowledgments need to be stressed, and one was missing:
How many pages are needed to repay Luca for one page (everybody knows which one)? Thanks again, not only for page x.
Andrea and Riccardo: I promised a full chapter of acknowledgments for you, but as you know I am late. So.. thanks a lot for allowing me to write the second edition!
I was forgetting .. thanks to Sogno Croato that always arrived and to Blasco that never left.

Bibliography

[1] R. E. Horton, Bull. Geol. Soc. Am. **56**, 275 (1945).

[2] A. N. Stralher, Geol. Soc. Am. **63**, 1117 (1952).

[3] L. B. Leopold and W. B. Langbein, U. S. Geol. Surv. Prof. Pap. **500-A**, (1962).

[4] A. E. Scheidegger, Bull. Assoc. Sci. Hydrol. **12**, 15 (1967).

[5] P. Meakin, J. Feder, and T. Jossang, Physica A **176**, 409 (1991).

[6] A. D. Howard, Water Resour. Res. **30**, 7261 (1994).

[7] K. Sinclair and R. C. Ball, Phys Rev. Lett. **76**, 3360 (1996).

[8] R. L. Leheny and S. R. Nagel, Phys. Rev. Lett. **71**, 1470 (1991).

[9] S. Kramer and M. Marder, Phys. Rev. Lett. **68**, 205 (1992).

[10] A. Maritan, A. Rinaldo, R. Rigon and I. Rodriguez-Iturbe , Phys. Rev. E **53**, 1501 (1996).

[11] M. Marsili, A. Maritan, F. Toigo, and J. R. Banavar, Review of Modern Physics, (to appear) (1996).

[12] A. Maritan, F. Toigo, J. Koplik, and J. R. Banavar, Phys. Rev. Lett **69**, 3193 (1992).

[13] J. M. Burgers, *The Nonlinear Diffusion Equation* (Riedel, Boston, 1974).

[14] F. Colaiori, A. Flammini, A. Maritan, and J. Banavar, submitted to Phys. Rev. E , (1996).

[15] I. Rodriguez-Iturbe, A. Rinaldo, R. Rigon, R. L. Bras and E. Ijjasz-Vasquez, Geophys. Res. Lett. **19**, 889 (1992).

[16] I. Rodriguez-Iturbe, A. Rinaldo, R. Rigon, R. L. Bras and E. Ijjasz-Vasquez, Water Resour. Res. **28**, 1095 (1992).

[17] A. Maritan, F. Colaiori, A. Flammini, M. Cieplak and J. R. Banavar, Science **272**, 984 (1996).

[18] S. A. Schumm, *The Fluvial System* (J. Wiley, New York, 1977).

[19] I. Rodriguez-Iturbe, R. L. Bras, E. Ijjasz-Vasquez, and D. G. Tarboton, Water Resour. Res. **28**, 988 (1992).

[20] D. G. Tarboton, R. L. Bras, and I. Rodriguez-Iturbe, Water Resour. Res. **24**, 1317 (1988).

[21] D. R. Montgomery and W. E. Dietrich, Nature **336**, 232 (1988).

[22] J. T. Hack, U. S. Geol. Surv. Prof. Paper **294-B**, (1957).

[23] B. B. Mandelbrot, *The Fractal Geometry of Nature* (Freeman, New York, 1983).

[24] I. R. Iturbe and A. Rinaldo, *Fractal River Basins: Chance and Self-Organization* (Cambridge Univ. Press., New York, in press, 1996).

[25] D. R. Montgomery and W. E. Dietrich, Science **255**, 826 (1992).

[26] J. S. Smaller, *Shock Waves and Reaction Diffusion Reaction* (Springer Verlag, New York, 1994).

[27] D. M. Gray, J. Geophys. Res. **66**, 1215 (1961).

[28] W. Langbein, .S. Geol. Surv. Prof. Paper **968-C**, 1 (1947).

[29] J. Muller, Geol. Soc. A Bull. **84**, 3127 (1973).

[30] A. Rinaldo, A. Maritan, F. Colaiori, A. Flammini, M. Swift, R. Rigon, J.R. Banavar and I. Rodriguez-Iturbe, submitted to Nature , (1996).

[31] L. B. Leopold and T. Maddock, U. S. Geol. Surv. Prof. **252**, 56 (1953).

[32] M. G. Wolman, U. S. Geol. Surv. Prof. **272**, 56 (1955).

[33] L. M. Brush, U. S. Geol. Surv. Prof. **282-f**, 1 (1961).

[34] L. B. Leopold, Am. J. Sci. **251**, 606 (1953).

[35] D. G. Tartobon, R. L. Bras, and I. Rodriguez-Iturbe, Parson Lab. Rep. no. 386 Dep. Civ. Eng. MIT Massachussetes 251 (1989).

[36] W. Thomson and P. Tait, *Treatise on Natural Philosophy* (PUBLISHER, Cambridge, 1878).

[37] A. Rinaldo, R. Rigon, R. L. Bras, and E. Ijjasz-Vasquez, Water Resour. Res. **28**, 1095 (1992).

[38] A. Rinaldo, Water Resour. Res. **28**, 2183 (1992).

[39] I. Rodriguez-Iturbe, A. Rinaldo, R. Rigon, R. L. Bras and Ijjasz-Vasquez, Geophys. Res. Lett. **19**, 889 (1992).

[40] D. A. Huse and C. L. Henley, Phys. Rev. Lett. **54**, 2708 (1985).

[41] M. Kardar, Phys. Rev. Lett. **55**, 2923 (1985).

[42] D. Fisher, Phys. Rev. Lett. **55**, 2924 (1985).

[43] D. G. Tartobon, R. L. Bras, and I. Rodriguez-Iturbe, Water Resour. Res. **24**, 1317 (1988).

[44] D. G. Tartobon, R. L. Bras, and I. Rodriguez-Iturbe, Water Resour. Res. **26**, 2243 (1990).

[45] I. Rodriguez-Iturbe, R. L. Bras, E. Ijjasz-Vasquez, and D. G. Tarboton, Water Resour. Res. **28**, 988 (1992).

[46] S. Lin, Bell Syst. Tech. J. 44, 2245 (1965).

[47] S. Lin and B. W. Kernighan, Oper. Res. **21**, 498 (1973).

[48] T. Sun, P. Meakin, and T. Jøssang, Phys. Rev. E **49**, 4865 (1994).

[49] T. Sun, P. Meakin, and T. Jøssang, Water Resour. Res. **29**, 1219 (1993).

[50] T. Sun, P. Meakin, and T. Jøssang, Phys. Rev. E **51**, 5393 (1995).

[51] M. V. von Smoluchowski, Phys. Z. **17**, 557 (1916).

[52] H. Takayasu, I. Nishikawa, and H. Tasaki, Phys. Rev. A **37**, 3110 (1988).

[53] H. Takayasu, M. Takayasu, A. Provata, and G. Huber, J. Stat. Phys. **65**, 725 (1991).

[54] S. N. Majumdar and C. Sire, Phys. Rev. Lett. **71**, 3729 (1993).

[55] T. M. Ligget, in *Interacting Particle Systems* (Springer-Verlag, ADDRESS, 1985), Chap. 15.

[56] D. Dhar and R. Ramaswamy, Phys. Rev. Lett. **63**, 1659 (1989).

[57] S. Zapperi, K. B. Lauritsen, and H. E. Stanley, Phys. Rev. Lett. **75**, 4071 (1995).

[58] H. Takayasu and I. Nishikawa, in *in Proc. 1st Int. Symp. for Science on Form.*, edited by S. Ishizaka (KTK Scientific, Tokio, 1986).

[59] L. Peliti, J. Phys. A. **19**, L365 (1986).

[60] P. Erdos and S. J. Taylor, Acta Math. Acad. Sci Hung. **11**, 137 (1960).

[61] G. H. Vineyard, J. Math. Phys. **4**, 1191 (1963).

[62] E. W. Montroll and G. H. Weiss, J. Math. Phys. **6**, 167 (1965).

[63] A. Maritan, J. R. Banavar, M. Cieplak, F. Colaiori, A. Flammini, A. Giacometti, A. Rinaldo and I. Rodriguez-Iturbe, in *in Proc. IXX Int. Conf. on Stat. Phys.*, edited by H. Bailin (World Scientific, Singapore, 1995).

[64] A. Rinaldo, A. Maritan, F. Colaiori, A. Flammini, R. Rigon, I. Rodriguez Iturbe and J.R. Banavar, Phys. Rev. Lett. **76**, 3364 (1996).

[65] M. Takayasu, H. Takayasu, and Y. H. Taguchi. Int. J. Mod. Phys. B **8**, 3387 (1994).

[66] P. Meakin and H. E. Stanley, J. Phys. A **17**, L173 (1984).